

Chapter 2

Chapter 2 :Many Particle Aspects of Graphene

The static structure factor, pair correlation function, self-energy, screening charge density, screened potential and compressibility has been investigated theoretically using both the density-density and spin density response functions of doped single graphene sheet based on the random phase approximation and on graphene's massless Dirac fermions concept. The local field effects have been considered in the simplistic Hubbard approximation. The static structure factor and pair correlation function are obtained by regularizing the dynamical polarization function, which otherwise is clearly divergent due to the interaction energy of the infinite Dirac sea of negative energy states. Ultraviolet wave vector cutoff has been used to exclude the effect of vacuum states. We find the structure factor to be dependent on the dimensionless coupling constant α , and for high values of coupling constant the magnetic structure factor indicates paramagnetic instability which is also corroborated from other theoretical investigations. The spin symmetric pair correlation function computed in the simplistic Hubbard approximation begins from zero at zero separation only at very high densities but the results for parallel spin and anti parallel spin pair correlation functions expose the short coming of this local field approximation. Our computed self energy of SLG sheet though displays a behaviour similar to that of 2DEG and BLG, its magnitude differs drastically from that of later two systems. Freidel oscillations are seen in computed screened potential and density of screening charge of graphene, which can be seen as a signature of Fermi liquid state in doped graphene. In agreement with experimental results, our computed pair distribution function, as a function of carrier density, suggests that exchange and correlation terms make negligible contribution to compressibility of

graphene. Incorporation of local field corrections reduces the magnitude of self energy, screening charge density and screened potential. This work should stimulate more investigations testing various other local field schemes and also quantum Monte Carlo based simulations.

2.1 Introduction

Many particle aspects play an important role in understanding low dimensional systems such as one dimensional electron gas (1DEG) and 2DEG etc., and obtaining ground state properties, excited states, relativistic effects, scattering theory of these systems. Interaction among many particle gives rise to some fascinating properties of a system like structure factor, pair correlation, self energy, exchange interaction and compressibility. These quantities for graphene qualitatively differ from normal 2DEG, observed in system like semiconductor heterostructures and MOSFETs. The approximate methods implemented to solve many particle aspects are Thomas-Fermi approximations (TFA), Random Phase Approximations (RPA), Improved RPA (IRPA), Singwi-Tosi-Land-Sjolander, Fermi liquid theory, Density Functional Theory (DFT) etc.

We have implemented one of the most widely accepted approaches i.e. the RPA. In this approximation it is assumed that only the single-particle excitations of the same wave vector as the Coulomb interaction plays an effective role in the screening process while the effects of others having different wave vectors cancel out. The RPA is more appropriate to use when the electron-electron interactions are strong enough that quantum coherence does not dominate.

A physical quantity of crucial utility in the understanding of the many body properties of condensed matter is the dynamic electron density-density response function χ , which has been briefly reviewed in Chapter 1. Many body properties like

ground state energy, electron-electron and transport scattering rate, collective excitations, compressibility, structure factor, pair correlation function etc are all calculated using this response function. This function for the peculiar case of graphene can be a function of one or all of the following parameters; wave vector \vec{q} , frequency ω , chemical potential μ ($\mu=0$ for intrinsic or undoped, $\mu\neq 0$ for extrinsic, doped or gated), temperature T , band gap Δ and disorder Γ), and has been calculated for various combinations of these parameters by a host of authors [1, 4-18].

Theoretical studies on graphene have established that transport and screening are considerably different from other conventional two dimensional electron gas (2DEG) systems. Also, unlike the 2DEG, in graphene, at low densities the effective velocity increases, the spin susceptibility is suppressed and the charge compressibility always remains positive, independent of the density [1, 2]. These peculiar features stem from the exchange interaction between electrons near the Fermi surface and electrons in the negative energy Dirac Sea. Another anomalous feature of graphene is that the electron-electron exchange and spin correlation is an increasing rather than decreasing function of carrier density [3]. In graphene even the vacuum state responds to an external potential and acts as a dielectric medium as the inter-band excitations are nearly similar to the virtual electron-hole excitations of a Dirac electron gas.

In this chapter, we consider with the dynamical polarization function of doped SLG in the wave-vector frequency domain $\chi_0(\vec{q}, \omega, \mu)$ at zero temperature and zero disorder, which has been obtained within RPA earlier [9,10]. This RPA polarization function for low energy excitation involving the graphene's π electron energy bands and having linear energy dispersion gives rise to the mass less Dirac fermions (MDF) concept. This RPA-MDF response function has been utilised in

various studies of graphene to obtain the ground state properties [17], screening [9,10], low frequency Plasmon excitations [12], the stopping and image forces on a moving charged particle [18], spin polarization [19], etc.

In the study of many body properties, a central role is played by the electron pair correlation function, $g(\vec{r})$. However, the results we obtain in this study on the many body properties of graphene are valid beyond the transport regime from where the correlation effects begin to play a noticeable role and therefore cannot be ignored. The $g(\vec{r})$ is an average distribution of electrons about any electron, and it is defined as the probability that another particle is at position \vec{r} if there is already one at $\vec{r}=0$ [20], and gives a suitable description for electron-correlation due to Coulombic repulsion that is the correlation hole. A suitable model pair-correlation function and static structure factor has its immediate relevance as its availability over a wide density range is crucial for new developments and applications of the density functional theory, through the construction of *ab initio* exchange and correlation energy functionals in generalized gradient approximations and in other beyond Linear density approximation schemes. A wealth of computational results on structure factor and pair correlation function from quantum Monte Carlo simulation studies for various systems have given a flip to resume and improve upon the study of these important functions and from time to time ingenious methods have been reported in obtaining expressions for this function [19]. For the case of graphene the pair correlation function has been worked out in ref.[21] and static structure factor in magnetic field has been obtained by Shiyuza [22].

Knowledge of ground state properties of a system is essential in understanding its basic physics and to make use of it for device making. Single-particle spectral function, associated mean free paths, quasiparticle properties, such

as inelastic quasiparticle lifetimes quasiparticle decay, renormalization factor, and renormalization velocity can be studied by knowing electron self-energy [23, 24]. Self-energy can also be used to obtain ARPES spectra which have been reported by a host of authors for graphene [25-27]. When a positive charge is placed in an electron gas, the electrons gather around the charge tries to compensate for the electrostatic potential it has induced. The phenomenon is known as screening and it is one of the simplest and most important manifestations of electron-electron interaction [28]. Because of reduced dimensionality and especially because of the semi-metallic nature of graphene's π -electron bands, the problem of screening of charged impurities remains open. In this context, various authors have reported calculations on screening, few of which include scattering treatment of Coulomb impurities embedded within the graphene plane [29,30]. Calculations on charged impurity screening in graphene with the use of vacuum polarization has received a huge attention because of its importance for transport properties and a general understanding of the theory of graphene. Static screening determines transport properties through screened Coulomb carrier scattering by charged impurities [6, 31]. The property of screening is also of interest for sensor applications of graphene in detecting atoms or molecules, which may be either absorbed on the upper surface of graphene or intercalated in the gap between the graphene substrate. It has been shown that within the RPA approach, screening of external charges by intrinsic graphene at zero temperature is characterized merely by a renormalization of graphene's background dielectric constant due to interband electron transitions [6,9,12,31,32]. The most common feature observed in screened potential is Friedel oscillations, which arise because of derivative discontinuity.

In an interacting electron system of uniform density, the inverse electronic compressibility is a fundamental physical quantity that is intimately related to the strength of inter-electron interactions. The compressibility of electron gas provides valuable information about the nature of the interacting ground state, particularly in the strong-coupling regime where (in addition to the exchange energy) Coulomb interaction energy also plays a dominant role. It also provides information about the chemical potential, stability of the system and so on. Change of local electrostatic potential and thereby change in local chemical potential of graphene was measured with the use of scanning single-electron transistor microscopy when the carrier density was modulated [33]. Observed results on local inverse compressibility were found to be quantitatively described by kinetic energy alone with the electron velocity renormalized by 10–15%. It has been speculated that the exchange and correlation energy contributions to compressibility either cancel each other out or are negligibly small. It has been argued that in SLG linear energy dispersion and chirality conspire to allow complete cancellation of exchange and correlation contributions just as was observed in the experiment [34]. This motivated us to compute pair distribution function as a function of carrier density, n to study the n – dependence of compressibility of graphene.

Many-body effects in SLG with zero gap and doping at zero temperature have been the subject of great interests [9, 31]. We evaluated structure factor, pair correlation function, self energy, density of screening charge, screened potential, compressibility using $\chi_0(\vec{q}, \omega)$ with and without LFC. This Chapter is organized in Four parts: Section 2.2 gives insight of the essential formalism. The computed results are discussed in Section 2.3. References are quoted in 2.4

2.2 Essential Formalism

In the case of 2D Dirac electrons interacting via the long range Coulombic potential on an hexagonal graphene sheet, the Hamiltonian is given by [14],

$$\mathcal{H} = \hbar v_F \sum_{\vec{k}} \psi_{\vec{k}}^\dagger \begin{pmatrix} -k_F & \phi_{\vec{k}}^* \\ \phi_{\vec{k}} & -k_F \end{pmatrix} \psi_{\vec{k}} + \sum_{\vec{q}} V_{\vec{q}} n_{\vec{q}}^\dagger n_{\vec{q}} \quad (1.1)$$

where $\phi_{\vec{k}} = k_x + ik_y$ and $\psi_{\vec{k}}$ is a two component field operator, k_F is the Fermi wave vector related to the chemical potential via $k_F = \mu/\hbar v_F$ $n_{\vec{q}}^\dagger = \sum_{\vec{k}} \psi_{\vec{k}+\vec{q}}^\dagger \psi_{\vec{k}}$ is the density operator, and

$$V_{\vec{q}} = 2\pi e^2/\epsilon_0 \vec{q} \quad (2.2)$$

is the 2D Fourier transform of the bare Coulomb interaction potential [14].

This effective Dirac-Weyl wave equation and the chirality of its eigenstates lead indeed to peculiar electron-electron interaction effects and unusual response to external potentials. Because of the band overlap of the wavefunctions obtained for the preceding Hamiltonian, the dynamical density response function is modified from the response function of the conventional 2DEG by a multiplicative factor of

$$f_{ss'}(\vec{k}, \vec{k}') = (1 + ss' \cos\theta)/2 \quad (2.2)$$

where $f_{ss'}(\vec{k}, \vec{k}')$ is the overlap of the band states, θ is the angle between \vec{k} and $\vec{k}' = \vec{k} + \vec{q}$, and $s, s' = \pm 1$ denote the band indices [6,10].

As mentioned in the introduction the quantity of interest for many body problems is the dynamical density-density response function which is needed to

describe the different approximations to Hamiltonian equation (2.1), since it determines the effective electron-electron interaction. The fluctuation dissipation theorem relates the imaginary part of the density-density response function with the structure factor [22]. The dynamic structure factor gives information on the relevant excitations of the ground state through the density operator [14].

2.2.1 The Structure Factor and pair distribution function

Using this response function the static regularised structure factor $S^R(\vec{q})$ and static regularised magnetic structure factor $\hat{S}^R(\vec{q})$ can be expressed, respectively, through the following relations [35,1];

$$S^R(\vec{q}) = \frac{-1}{n\pi} \int_0^\infty d\omega \text{Im}\{\delta\chi(\vec{q}, \omega)\} \quad (2.4)$$

$$\hat{S}^R(\vec{q}) = \frac{1}{n\pi g^2 \mu_B^2} \int_0^\infty d\omega \text{Im}\{\delta\chi^s(\vec{q}, \omega)\} \quad (2.5)$$

$\text{Im}\{\delta\chi(\vec{q}, \omega)\}$ and $\text{Im}\{\delta\chi^s(\vec{q}, \omega)\}$ are the regularized imaginary part of the dynamic density-density and dynamic spin-density response functions, respectively, defined as [26-27];

$$\delta\chi(\vec{q}, \omega) = \frac{\delta\chi_0(\vec{q}, \omega)}{1 + V_s^{eff}(\vec{q})\delta\chi_0(\vec{q}, \omega)} \quad (2.6)$$

$$\delta\chi^s(\vec{q}, \omega) = -g^2 \mu_B^2 \frac{\delta\chi_0(\vec{q}, \omega)}{1 + V_a^{eff}(\vec{q})\delta\chi_0(\vec{q}, \omega)} \quad (2.7)$$

With

$$\delta\chi_0(\vec{q}, \omega) = \left[\chi_0(\vec{q}, \omega) - \chi_0(\vec{q}, \omega)|_{E_f=0} \right] \quad (2.8)$$

The regularized irreducible polarization function has been obtained by subtracting vacuum irreducible polarization $\chi_0(\vec{q}, \omega)|_{E_f=0}$ from $\chi_0(\vec{q}, \omega)$, the temperature independent irreducible dynamic polarization function of doped graphene [2], $g\mu_B$ is the magnetic moment of an electron; g is the Lande factor and μ_B is the Bohr magneton, $V_s^{eff}(\vec{q})$ and $V_a^{eff}(\vec{q})$ are the symmetric and anti-symmetric spin effective potentials respectively given by the following equations [35,36];

$$V_s^{eff}(\vec{q}) = V_{\vec{q}}[1 - G(\vec{q})] \quad (2.9)$$

$$V_a^{eff}(\vec{q}) = V_{\vec{q}}G^s(\vec{q}) \quad (2.10)$$

Where

$$G(\vec{q}) = V(\sqrt{q^2 + k_F^2})/2V_{\vec{q}} \quad (2.11)$$

and

$$G^s(\vec{q}) = -V(\sqrt{q^2 + k_F^2})/2V_{\vec{q}} \quad (2.12)$$

are the static LFC for the density-density and spin density fluctuations, respectively, in the Hubbard approximation [35].

The regularization is done to make the integrals converge as $\chi_0(\vec{q}, \omega)$ increases with \vec{q} at large \vec{q} and falls like ω^{-1} at large ω . The divergence is expected because the response function includes the vacuum fluctuations of the infinite sea of negative particles [1]. The non-zero vacuum weight is a relativistic signature of

graphene and is a consequence of particle-antiparticle pair creation or the Dirac Sea. By this renormalization procedure we have the chemical potential of undoped graphene as our zero of energy, and now the ω integrals are finite.

The RPA is a many body theoretic method by which quantitative predictions beyond the Hartree-Fock model can be made. And though it is very successful in describing many properties nevertheless has its shortcoming, one of which is that it misses to accommodate the local field effects due to electronic exchange and correlation. The electron-electron correlation and exchange effect beyond the RPA is taken into account by incorporating a term containing the local field corrections in the effective potential.

The Fourier transform of static structure factor and magnetic structure factor give the spin-symmetric $g(\vec{r})$ and spin anti symmetric $\hat{g}(\vec{r})$, pair correlation functions respectively, which for the case of graphene can be written as follows [35,36];

$$g(\vec{r}) = 1 + \frac{1}{n} \int_0^\beta \int_0^{2\pi} \frac{\vec{q} d\vec{q} d\theta}{(2\pi)^2} \cos(\vec{q} \cdot \vec{r}) [S^R(\vec{q}) - 1] \quad (2.13)$$

$$\hat{g}(\vec{r}) = \frac{1}{n} \int_0^\beta \int_0^{2\pi} \frac{\vec{q} d\vec{q} d\theta}{(2\pi)^2} \cos(\vec{q} \cdot \vec{r}) [\hat{S}^R(\vec{q}) - 1] \quad (2.14)$$

where \vec{r} is the radial distance. The double integral in Equations (2.13) & (2.14) over the other variable \vec{q} is divergent, for which we introduce an ultra violet wave vector cut off k_a , which becomes necessary to make quantitative predictions for the peculiar case of graphene [1, 21]. The dimensionless parameter β is defined as k_a/k_F where k_a is determined in a way so as to keep the number of states in the Brillouin zone fixed, that is, $\pi k_a^2 = (2\pi)^2/A_0$, in which $A_0 = 3\sqrt{3}a_0^2/2$ is the area

of the unit cell in the honeycomb lattice and $a_0 = 1.42\text{\AA}$ is the carbon-carbon distance [3].

The $g(\vec{r})$ and $\hat{g}(\vec{r})$ can be written as a combination of parallel spin correlation function $g \uparrow\uparrow(\vec{r})$ and anti-parallel spin pair correlation function $g \uparrow\downarrow(\vec{r})$, as under [35, 36];

$$g \uparrow\uparrow(\vec{r}) = g(\vec{r}) + \hat{g}(\vec{r}) \quad (2.15)$$

$$g \uparrow\downarrow(\vec{r}) = g(\vec{r}) - \hat{g}(\vec{r}) \quad (2.16)$$

For a 2D system, self-energy $E^{sl}(\mathbf{k})$, density of screening charge, $n_s(\mathbf{r})$ and Screened potential, $V_{SCR}(\mathbf{r})$ can be given by [35].

2.2.2 Self Energy

$$E^{sl}(k) = 2 \int_0^{k_f} \int_0^{2\pi} \frac{1}{4\pi^2} \frac{V_{\vec{q}}}{\epsilon(|\mathbf{k}-\mathbf{k}'|)} k' dk' d\theta \quad (2.17)$$

2.2.3 Screening Charge Density and Screened Potential

$$n_s(r) = \frac{Ze}{4\pi^2} \int_0^\infty \int_0^{2\pi} e^{i\vec{q}\cdot\vec{r}} \left[1 - \frac{1}{\epsilon(q)}\right] q dq d\theta \quad (2.18)$$

$$V_{SCR}(r) = \frac{Ze}{4\pi^2} \int_0^\infty \int_0^{2\pi} e^{i\vec{q}\cdot\vec{r}} \left[\frac{V_{\vec{q}}}{\epsilon(q)}\right] q dq d\theta \quad (2.19)$$

Equation 2.17 has been obtained by replacing \vec{q} by $|\mathbf{k} - \mathbf{k}'|$ in $V_{\vec{q}}$ and $\epsilon(q, \omega = 0)$ respectively.

2.2.4 Compressibility

We have computed pair distribution function as a function of n to study the n – dependence of compressibility of graphene. The compressibility can be defined by $k^{-1} = \partial^2 \epsilon / \partial n^2$, where energy per particle functional, ϵ can be expressed in terms of

kinetic energy per particle, t_0 , Coulomb potential, V_{coul} , pair correlation function, $g(\vec{r})$ as follows [37];

$$\frac{\partial^2 \varepsilon}{\partial n^2} = \frac{\partial^2 t_0}{\partial n^2} + 2 \int d\vec{r} V_{\text{coul}} \frac{\delta g(\vec{r})}{\delta n} + n \int d\vec{r} V_{\text{coul}} \frac{\left(\frac{\delta g(\vec{r})}{\delta n}\right)}{\delta n} \quad (2.20)$$

$g(r, z)$ for graphene can be given by

$$g(r, z) = 1 + \frac{1}{2n\pi} \int_0^{k_a} q J_0(qr) [S(q, z) - 1] dq \quad (2.21)$$

Where $n = z \times 10^{14} \text{ cm}^{-2}$.

$S(q, z)$ is static structure factor.

$E^{sl}(k)$, $n_s(r)$ and $V_{SCR}(r)$ has been also evaluated including local field effects.

2.3 Results and Discussions

2.3.1 The Structure Factor and Pair Distribution function

The properties of the Dirac electrons are defined in terms of a dimensionless density independent coupling constant $\alpha (= r_s) = g_0 e^2 / v_F \varepsilon_0 \hbar$ in which $g_0 = g_s g_v = 4$ is the product of spin and valley degeneracy, ε_0 is the average dielectric constant of the substrate and air and its value lies between 1 and 2 for SiC or SiO₂ substrate [3]. This coupling constant is the ratio of a typical Coulomb energy to the hopping energy and is similar to the r_s parameter defined for the case of usual non relativistic 2DEG of finite mass electrons, and is a measure of the strength of Coulombic attraction. It depends only on material properties and environmental conditions and it is the measure of the strength of the Coulombic attraction. α is also used to characterize the ratio of coulomb interaction and band energy scales in graphene. The typical value of the coupling constant for graphene supported on SiC

or SiO₂ substrate is also 1 or 2, but in some studies investigations have also been done keeping larger coupling constants values of around 3 & 4 [38]. The dielectric constant in graphene is a tuneable parameter which stems from the peculiar screening properties of graphene. The screening in graphene is a combination of metallic screening due to intra-band transition and insulating screening due inter band transition (which is absent in conventional 2DEG) leading two overall strange screening properties all of which can be traced back to the chiral relativistic nature of graphene [10].

We worked out the static structure factor in terms of the following scaled parameters; $x=|\vec{q}|/k_F$ and $y=\hbar\omega/E_f$. In the long wavelength limit, for $y < x$, we obtain an analytical expression for the static structure factor without incorporating the LFC;

$$S_A(x \rightarrow 0) = \left(\frac{x^3}{\pi\alpha^2}\right) \ln \left\{1 + \frac{\alpha^2}{(x+\alpha)^2}\right\} \quad (2.22)$$

We subtract from this equation the analytical structure factor obtained from the expression for spectral weight derived in the RPA for the graphene vacuum, given by [14];

$$S_A^V(x) = \left(\frac{x^4}{32\pi\alpha^2}\right) \quad (2.23)$$

which represents a collection of intra-band particle-hole transitions, to get the regularised structure factor in the long wavelength limit;

$$S_A^R(x) = [S_A(x \rightarrow 0) - S_A^V(x)] \quad (2.24)$$

In the case of graphene the f -sum rule, that determines the conservation of the particle number gives an infinite contribution due to the vacuum energy and therefore is of no physical significance as such. The contribution from the lower filled band calls for an energy cut-off limit for the sum rule to be applicable and therefore to represent a real response of the system, as has been elaborately discussed in Ref.14.

In Figure 2.1, we plot the computed dynamic structure factor or spectral weight for undoped and doped SLG at $x=1$. Curve A is for doped SLG and Curve B for undoped one. From the figure it is quite conspicuous that the Curve A exhibits a peak while curve B does not turns up with any peak. The curve B remains zero up to $x < 1$ and thereafter shows a finite value. It is well known that the undoped SLG there is no plasmon mode at zero temperature, since in an intrinsic (undoped) SLG the net electron density is zero and therefore Fermi energy is zero. However, at finite temperatures or when spin orbit interactions are included plasma oscillations can occur as well in undoped graphene. The curve A for doped SLG displays a peak which is a clear cut evidence for the existence of collective excitations in this 2D nanostructure.

If we simply plot the structure factor without regularising the response function we see that the structure factor grows with increasing values of x , $S(x) \rightarrow \infty$ as $x \rightarrow \infty$ (figure 2.2 - Curves A and B), because of the contribution of the vacuum energy, in contrast to the normal observed behaviour $S(x) \rightarrow 1$ as $x \rightarrow \infty$, of non relativistic electron gas - and for the particles on a lattice this behavior denotes the absence of short range particle correlations. This novel behavior like other peculiar aspects of graphene is well attributed to the relativistic nature of mass-less quasiparticles. In SLG the dielectric medium is few of virtual particle-hole pairs and

this ascending value of $S(x)$ for increasing x is a result of pair creation at short distances. It has been pointed out that an experimental determination of the vacuum spectral weight via the inelastic light scattering will be a clear signal of the quantum nature of the graphene vacuum state [22]. Therefore to suppress the effect of vacuum polarization we adopt the regularisation procedure as discussed above. The regularised dimensionless analytical static structure factor from equation (2.24) is plotted for four different values of coupling constants in figure 2.3. The small x behaviour of $S(x)$ is important because it determines the oscillation-averaged long range part of pair correlation function [39].

From the figure 2.3, we observe that $S_A^R(x)$ shows a hump and at $S_A^R(x \rightarrow 0)$, it tends to zero, which is a manifestation of the conservation principle for the number of particles. For increasing values of coupling constant the hump translates with momentum. In the other limit, that is for increasing values of x we notice that $S_A^R(x)$ goes to zero again, which means that $S_A^R(x)$ is governed by the vacuum spectral weight for higher values of x and which is unrealistic as this expression is valid for small values of x . The computed numerical dimensionless structure factor from equation (2.2) incorporating the LFC is plotted in figure 2.4 for four different values of coupling constants. Here the structure factor shows a hump with a maximum value of about 0.275 for $\alpha=1$, which is almost double of that observed for the case of analytical structure factor, and thereafter it saturates for increasing x . For increasing coupling strength values that is; $\alpha=2, 3$ & 4 , the maximum value of the hump diminishes and also it shifts and broadens, with a larger saturation value for $\alpha=2$, but for $\alpha=3$ & 4 , it is observed that the curve begins to grow with increasing x . As far as the magnitude of saturation value is concerned the $S^R(x)$ fails to recover the standard behaviour $S^R(x) \rightarrow 1$, observed for non-relativistic electrons. Figure 2.5

shows the computed $S^R(x)$ without LFC. Here we notice an enhanced saturation value for $\alpha=1$, but the curves begin to grow faster with x than compared to that in figure 2.4 and from coupling value of $\alpha=2$ itself.

In figure 2.6 we plot the magnetic structure factor for four different values of the coupling constants. This behaviour of the regularised structure factor is very similar to the subtracted structure factor reported in Ref.22. The following features noted in Ref.22 is also seen here for $\hat{S}^R(x)$ that is, (a); $\hat{S}^R(x) \rightarrow 0$ for $x \rightarrow 0$, (b) $\hat{S}^R(x) \rightarrow 0$ as $x \rightarrow \infty$, which means that for increasing x the contribution due to polarization vacuum energy is dominant, (c) $\hat{S}^R(x)$ shows a broader hump than $S^R(x)$ about the value 0.275 for $\alpha=1$ however with increasing coupling strength the trend is reversed from that observed for $S^R(x)$, that is $\hat{S}^R(x)$ begins to increase with $\alpha=2$. A new striking feature that appears in our study in the case of $\hat{S}^R(x)$ in contrast to the $S^R(x)$ behaviour is the observation of sharp peaks with enhanced value of about 1.3 for $\alpha=3$ & 4. The peaks observed are indicative of paramagnetic instability and this corroborates with the findings in Ref.37, where it is reported that exchange interactions between Dirac Fermions evaluated in the Hartree-Fock model can stabilize a ferromagnetic phase at low doping when the coupling is sufficiently large.

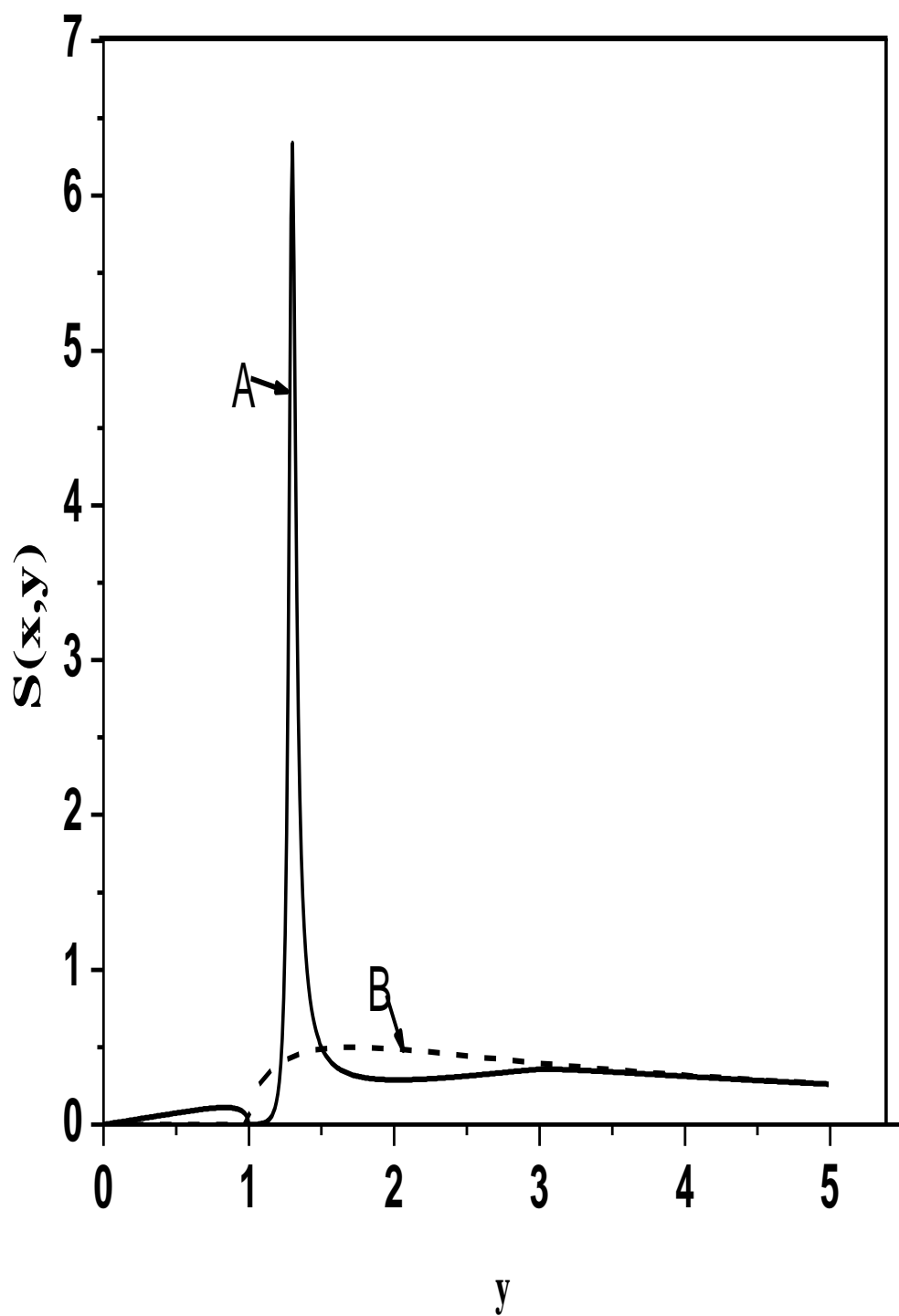


Figure 2.1 Plot of $S(x,y)$ At $x=1$. Solid curve A for doped graphene and dotted curve B for undoped graphene.

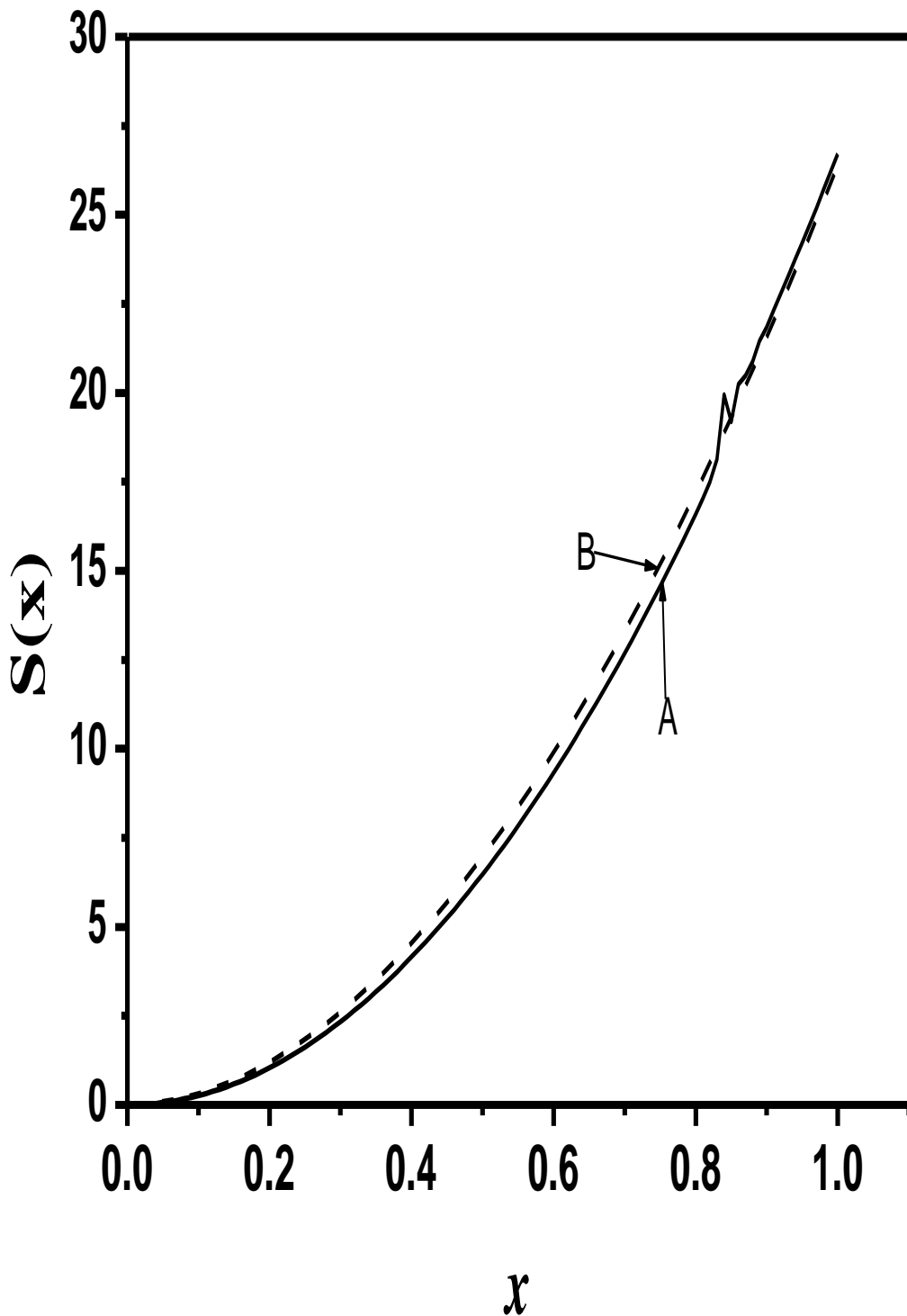


Figure 2.2 Plot of $S(x)$ vs x : Solid curve A for doped graphene and dotted curve B for undoped graphene.

However in contrast to this prediction the RPA low density calculation involving both exchange and correlation has ruled out a spontaneous magnetic phase transition even at large coupling constants [40]. In the Hubbard approximation for the LFC, which we have used, only spin exchange interaction is considered and the contribution due to electron-electron correlation interaction is zero, hence the conformity of the predictions between us and Ref.38. These contradicting predictions beckon experimental investigations to check whether graphene supports any form of ferromagnetism. However, the results we have obtained on the static structure factor can be used to calculate the exchange energy per electron of the graphene in the electric potential created by its own exchange hole and the electron-electron correlation energy. And by a familiar strategy of integration of the structure factor by combining with another coupling constant our results can be used to obtain the interaction energy contribution to Helmholtz free energy or the thermo dynamical potential of the 2D Dirac electron gas [36]. Besides the results can be of interest in building beyond linear density approximation exchange-correlation energy density functionals and also the magnetic response of the 2D Dirac electron gas.

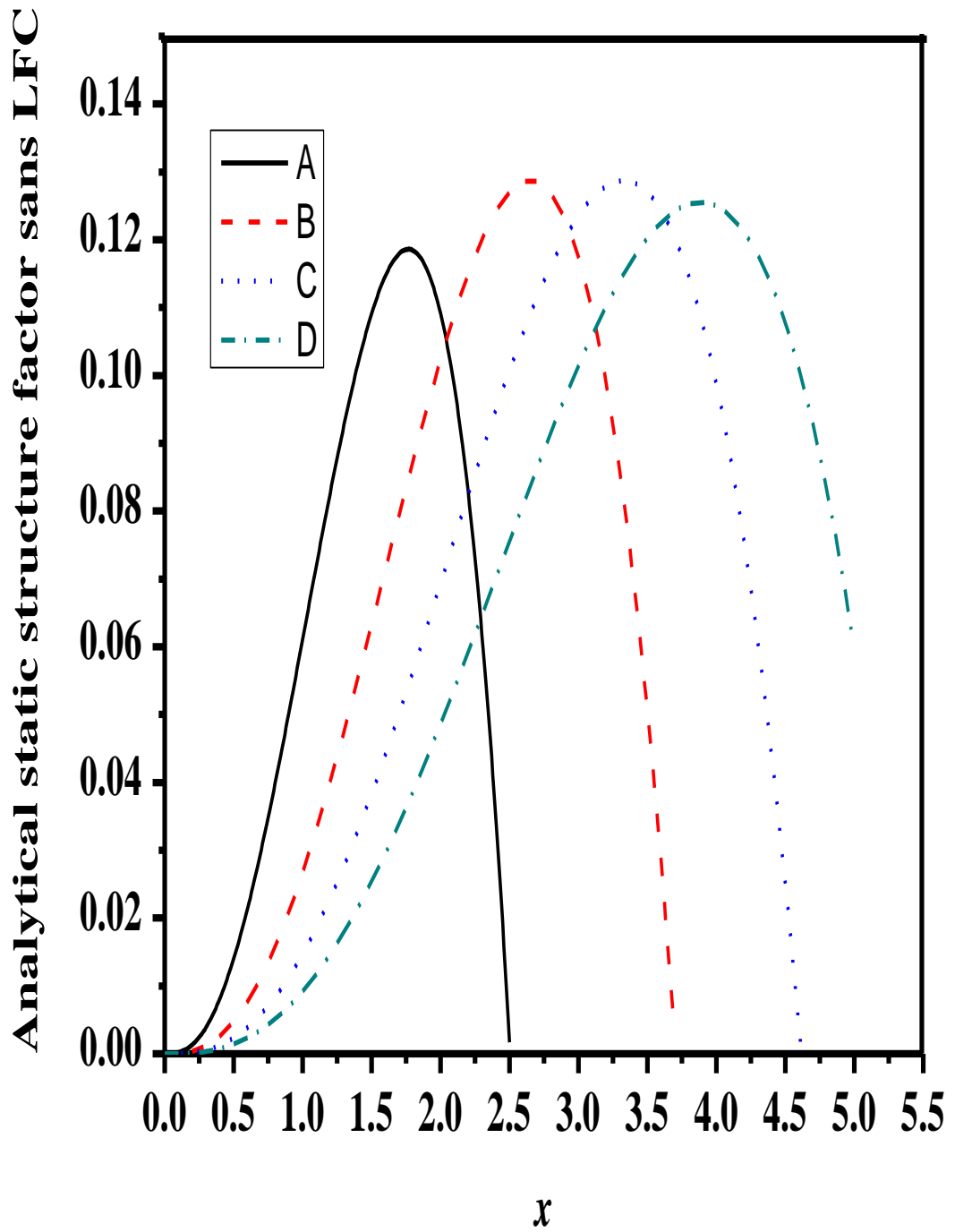


Figure 2.3 Static dimensionless long wavelength limit regularised analytical structure factor, $S_A^R(x)$ vs x , sans LFC, plotted in the curves A, B, C & D, for dimensionless coupling constants $\alpha = 1, 2, 3$ & 4 , respectively.

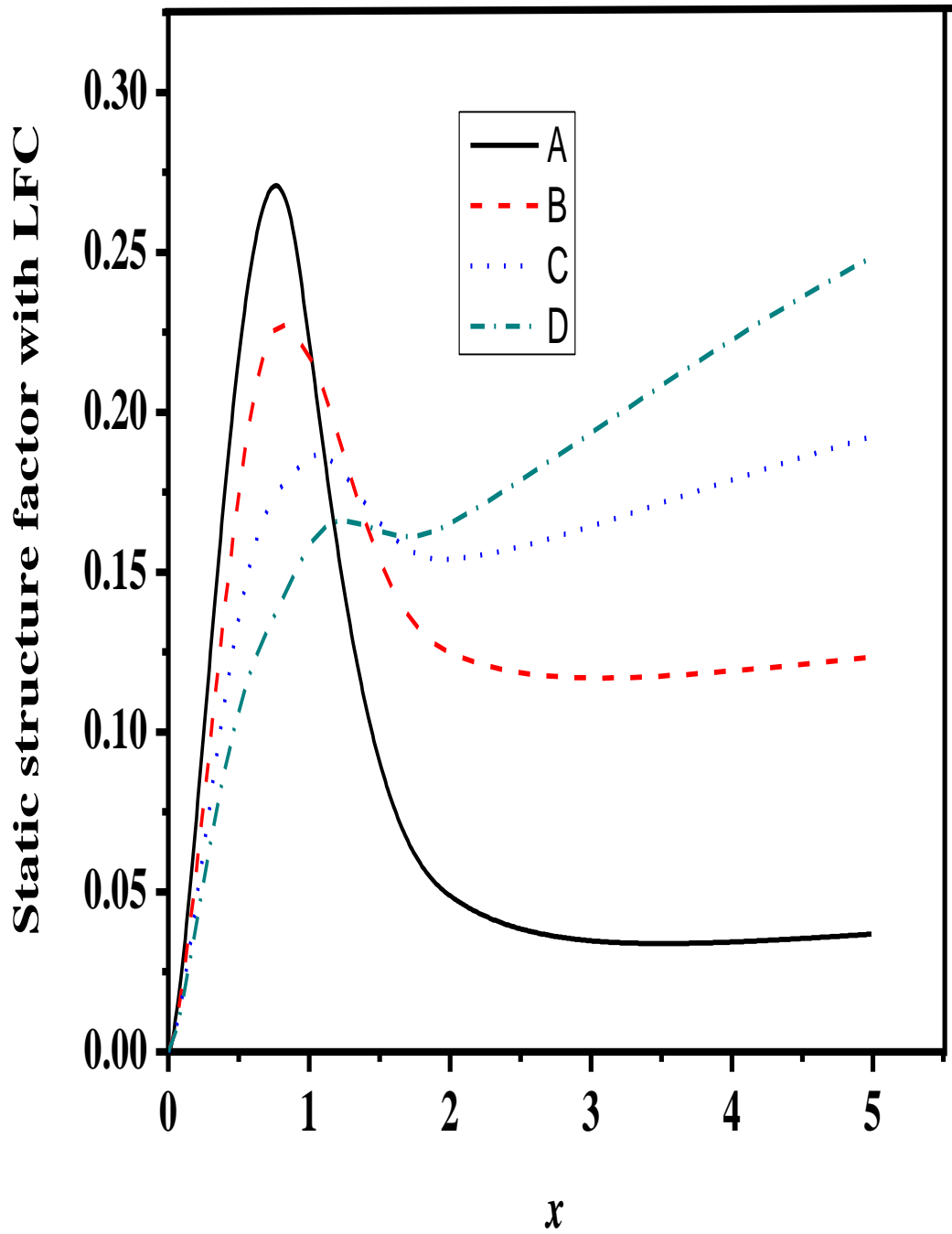


Figure 2.4 Static dimensionless regularised structure factor, $S^R(x)$ vs x , with LFC, plotted in the curves A, B, C & D, for dimensionless coupling constants $\alpha = 1, 2, 3$ & 4 , respectively

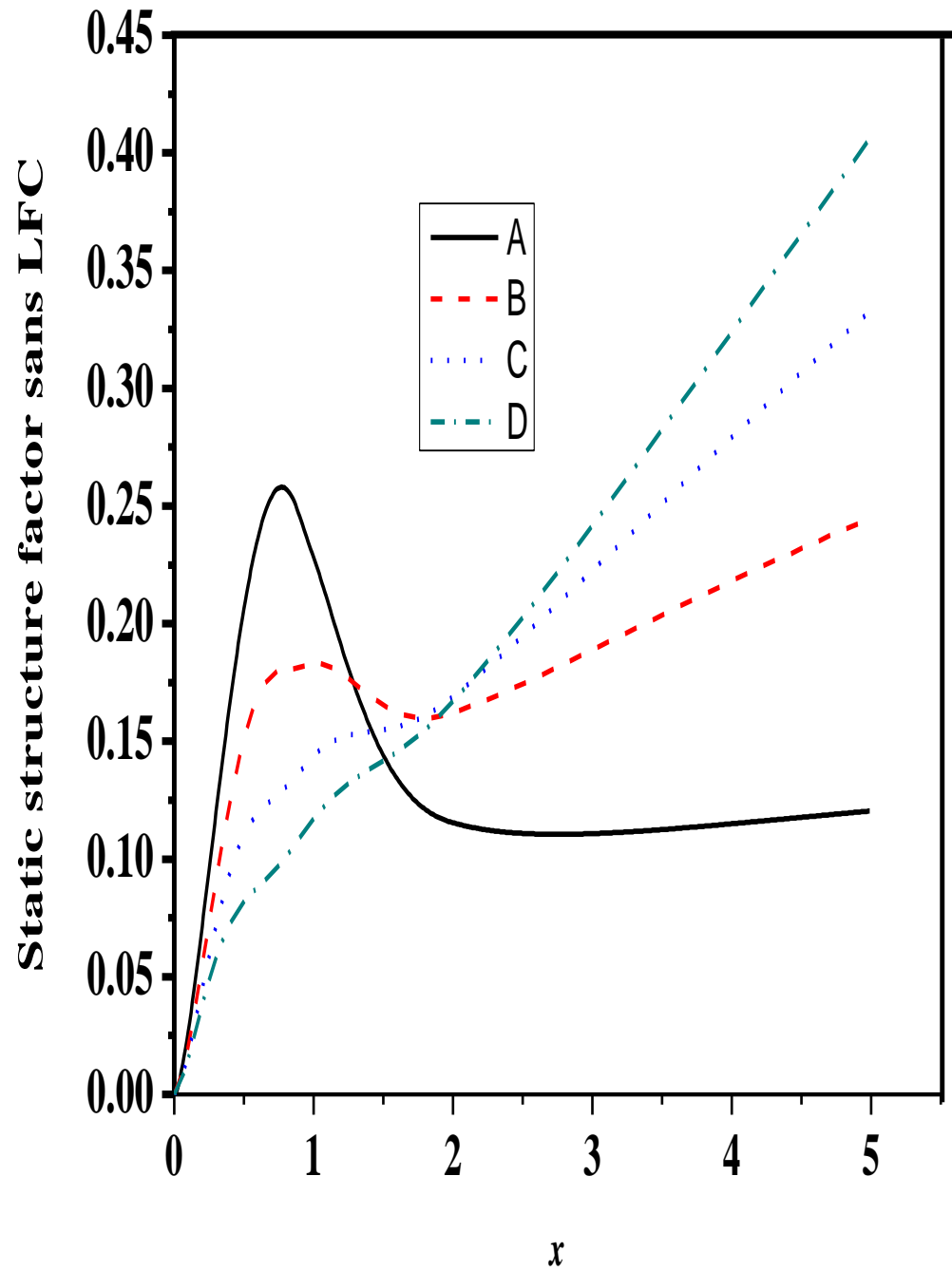


Figure 2.5 Static dimensionless regularised structure factor, $S^R(x)$ vs x , sans LFC, plotted in the curves A, B, C & D, for dimensionless coupling constants $\alpha = 1, 2, 3, \& 4$, respectively.

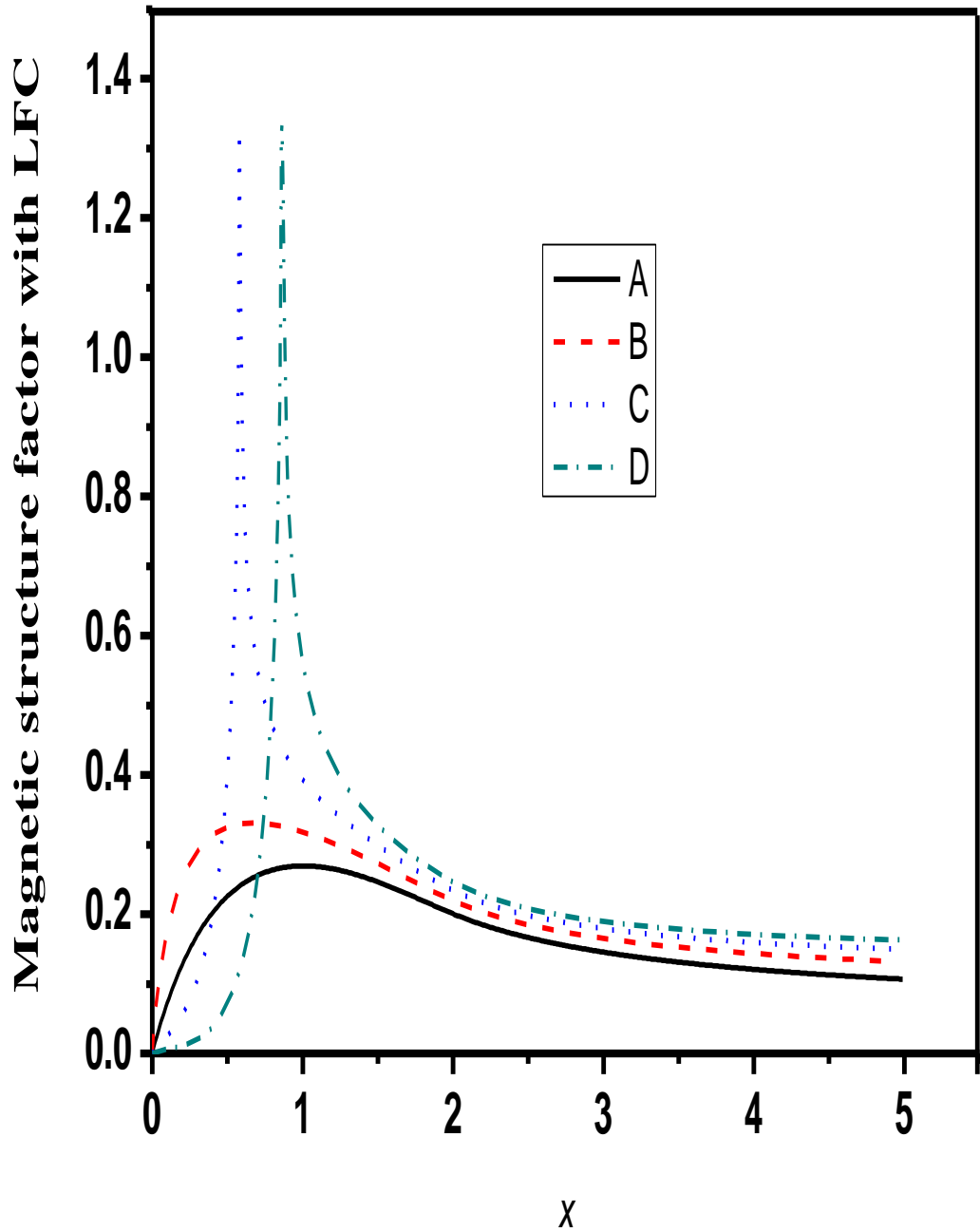


Figure 2.6 Magnetic static dimensionless regularised structure factor, $\hat{S}^R(x)$ vs x , with LFC, plotted in the curves A, B, C & D, for dimensionless coupling constants $\alpha = 1, 2, 3$ & 4 , respectively.

From the results of the structure factor we computed the pair correlation functions from equations (2.13)-(2.16). The cut off parameter β may be written in terms of the coupling constant α and electron density n as; $\beta = \sqrt{\alpha/nA_0}$. The value of β is small in heavily doped samples and is large for lighter systems. The symmetric spin pair correlation function from equation (2.13) is plotted in Figure 2.7 with LFC and in figure 2.8 sans LFC. It is known that the RPA gives grossly unphysical result for the pair correlation function which deteriorates further for low dimensional systems [41]. For graphene in this Hubbard approximation the pair correlation function is found to be sensitively dependent on the cut off parameter. We observe that for low densities which corresponds to high cut off value of the parameter β , the spin symmetric pair correlation function yields negative values at zero separation. But when the density is enhanced such that $\beta \cong 2.1785$ which correspond to $n \cong 8.04 \times 10^{14} \text{cm}^{-2}$ at $\alpha = 2$, the $g(\vec{r})$ gets rid of negative value for higher coupling strengths. But for small coupling strength of $\alpha = 1$ it begins with a slightly negative value as can be noticed from figure 2.7. In figure 2.8 the trend observed in figure 2.7 is reversed, however only a small difference of values of the four curves at $x=0$ is seen. The parallel spin pair correlation functions from equation (2.15) with and without LFC are plotted in figures 2.9 & 2.10, respectively. And the anti parallel spin pair correlation functions from equation (2.16) is depicted in figures 2.11 & 2.12, respectively. The $g_{\uparrow\uparrow}(\vec{r})$ with LFC plotted in figures 2.9 turns up with a negative unphysical value of about -0.9 for $\alpha = 1$ at $x=0$, which slightly improves for increasing α . The situation worsens when $g_{\uparrow\uparrow}(\vec{r})$ is plotted without LFC in figure 2.10, as is the case with RPA, but here it is seen that all the curves for different α merge together. Similarly the $g_{\uparrow\downarrow}(\vec{r})$ shown in figure 2.11 begins with a little unrealistic positive value of 0.87 which improves with increasing α , and for $\alpha = 4$ it

better to 0.79. Similar to the case of figure 2.10 the situation deteriorates when $g_{\uparrow\downarrow}(\vec{r})$ is computed sans LFC as displayed in figure 2.12. The computational results of both $g_{\uparrow\uparrow}(\vec{r})$ & $g_{\uparrow\downarrow}(\vec{r})$ expose the shortcoming of Hubbard approximation. It remains to be seen whether this deficiency in the Hubbard LFC scheme can be overcome with some other static or dynamical LFC methods. Also it is envisaged that this work will stimulate further studies in this regard through self-consistent computing schemes and also quantum Monte Carlo simulation based investigations to obtain the pair correlation function for graphene.

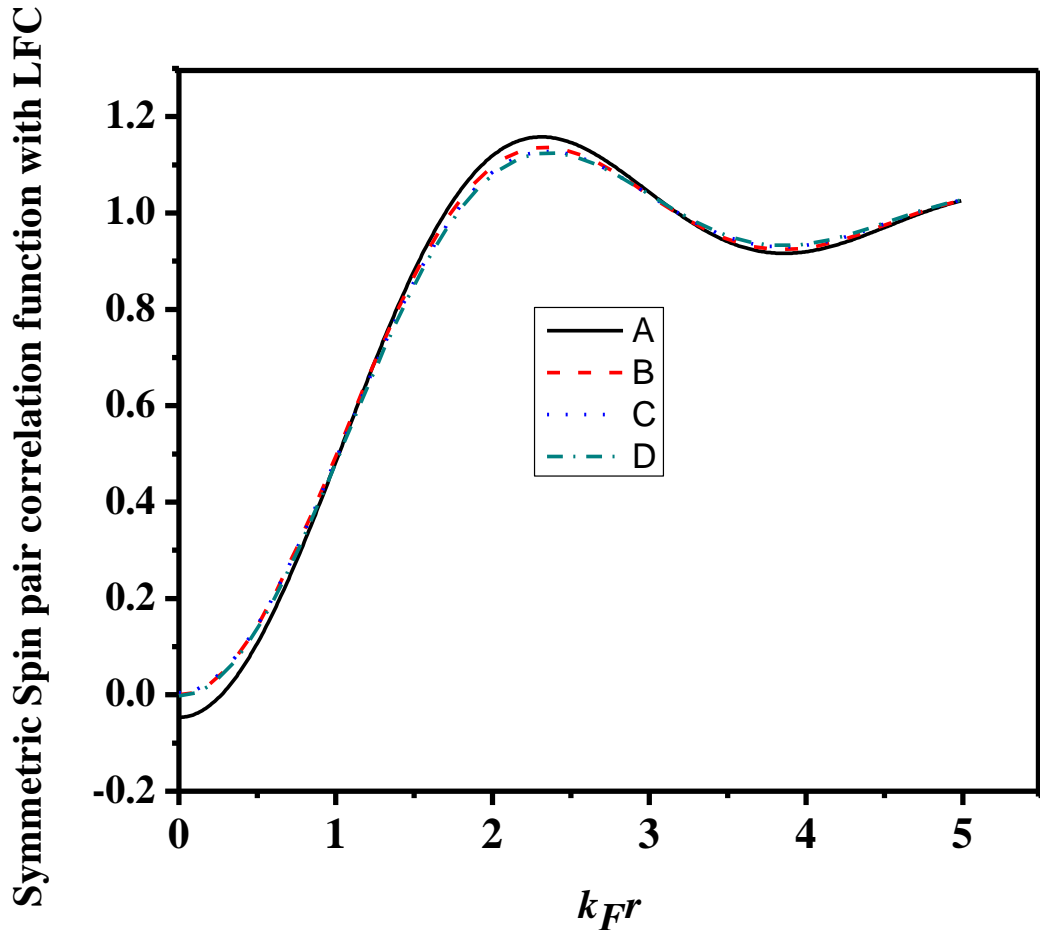


Figure 2.7 Spin symmetric dimensionless regularised pair correlation function, $g(k_F \vec{r})$ vs $k_F \vec{r}$, with LFC, in the curves A, B, C & D, for dimensionless coupling constants $\alpha = 1, 2, 3$ & 4 , respectively.

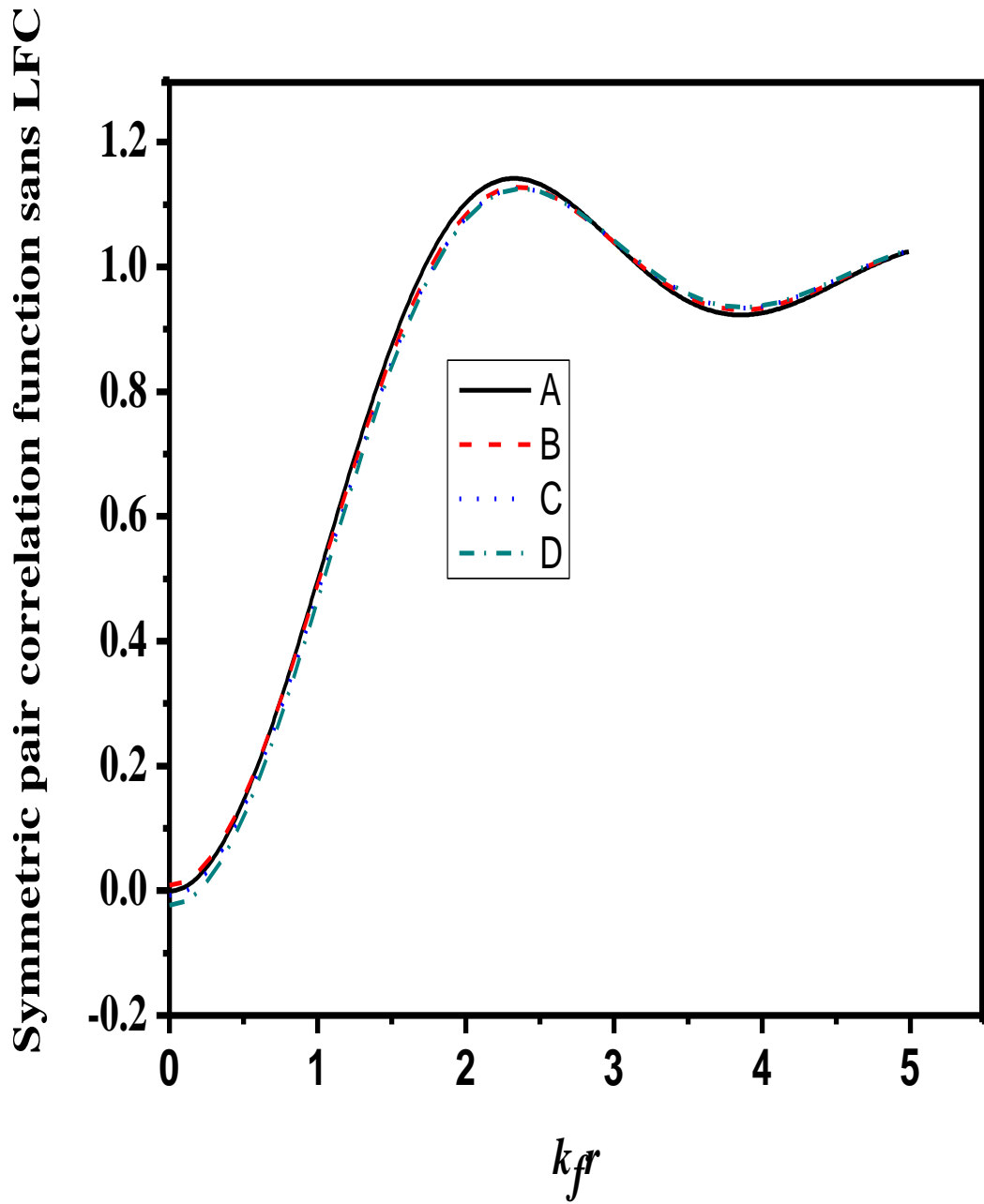


Figure 2.8 Spin symmetric dimensionless regularised pair correlation function, $g(k_F \vec{r})$ vs $k_F r$, sans LFC, in the curves A, B, C & D, for dimensionless coupling constants $\alpha = 1, 2, 3$ & 4 , respectively.

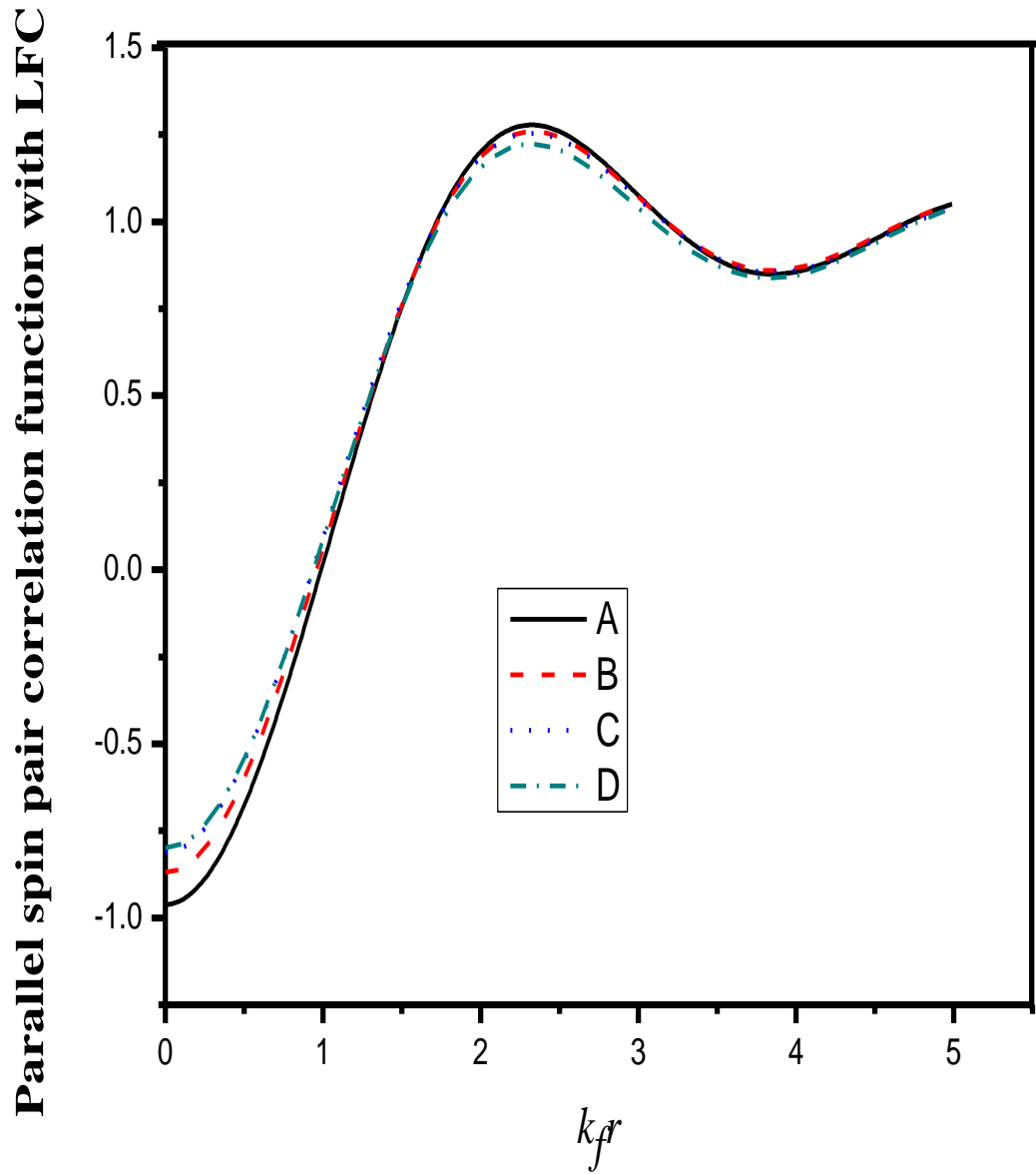


Figure2.9 Parallel spin dimensionless regularised pair correlation function, $g_{\uparrow\uparrow}(k_F \vec{r})$ vs $k_F \vec{r}$, with LFC, in the curves A, B, C & D, for dimensionless coupling constants $\alpha = 1, 2, 3$ & 4 , respectively.

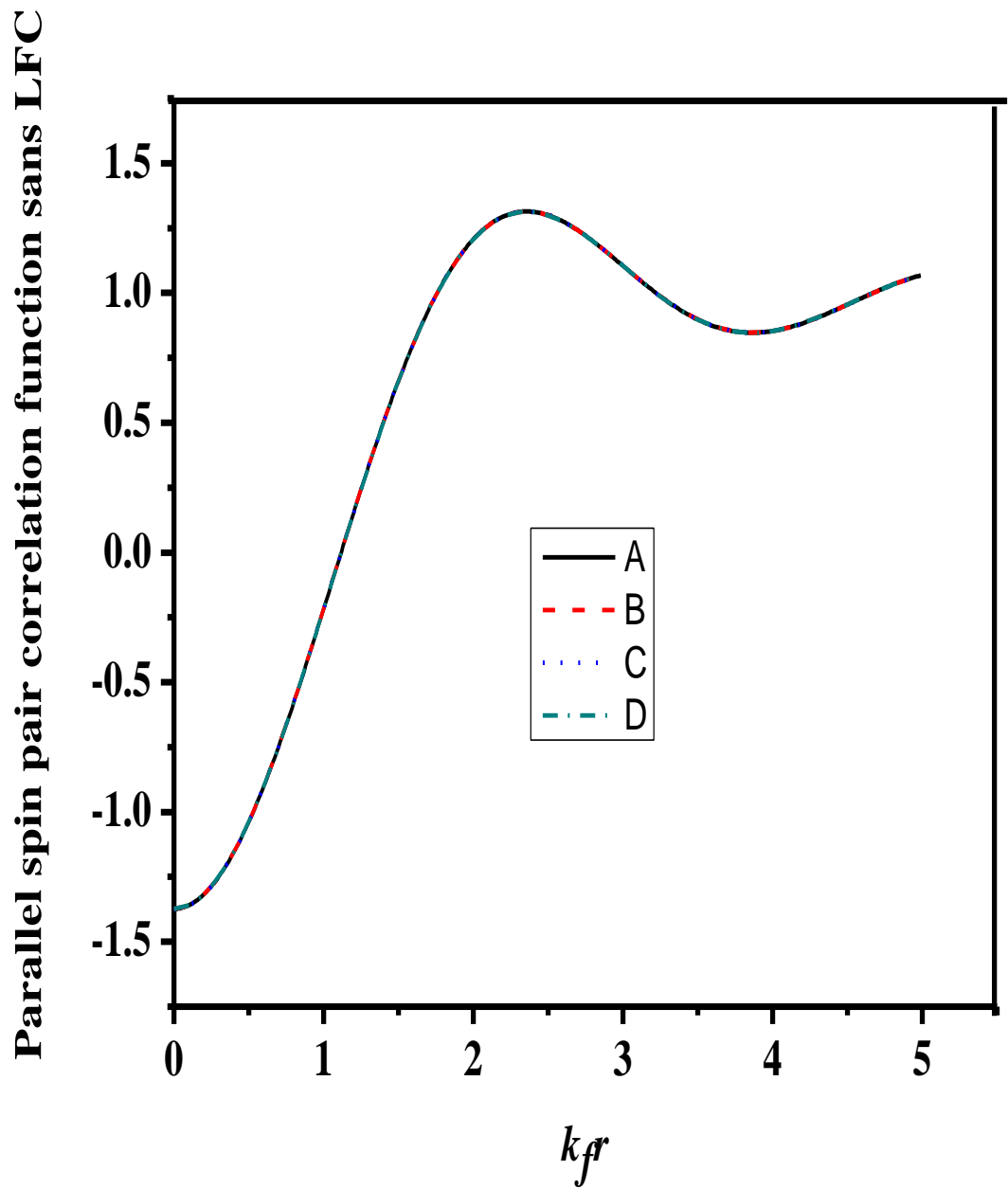


Figure 2.10 Parallel spin dimensionless regularised pair correlation function, $g_{\uparrow\uparrow}(k_F \vec{r})$ vs $k_F r$, sans LFC, in the curves A, B, C & D, for dimensionless coupling constants $\alpha = 1, 2, 3$ & 4 , respectively

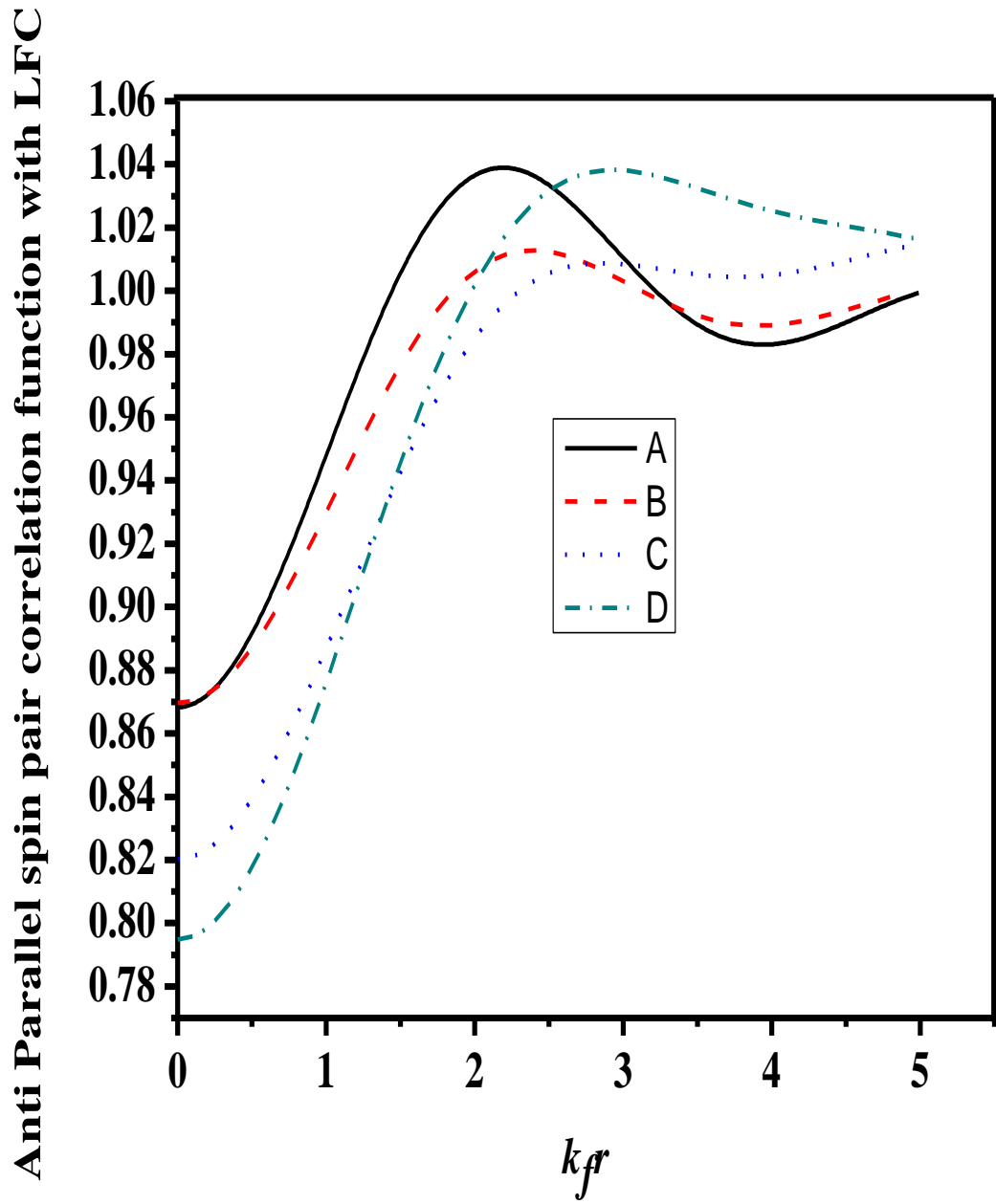


Figure 2.11 Anti parallel spin dimensionless regularised pair correlation function, $g_{\uparrow\downarrow}(k_F \vec{r})$ vs $k_F \vec{r}$, with LFC, in the curves A, B, C & D, for dimensionless coupling constants $\alpha = 1, 2, 3$ & 4, respectively.

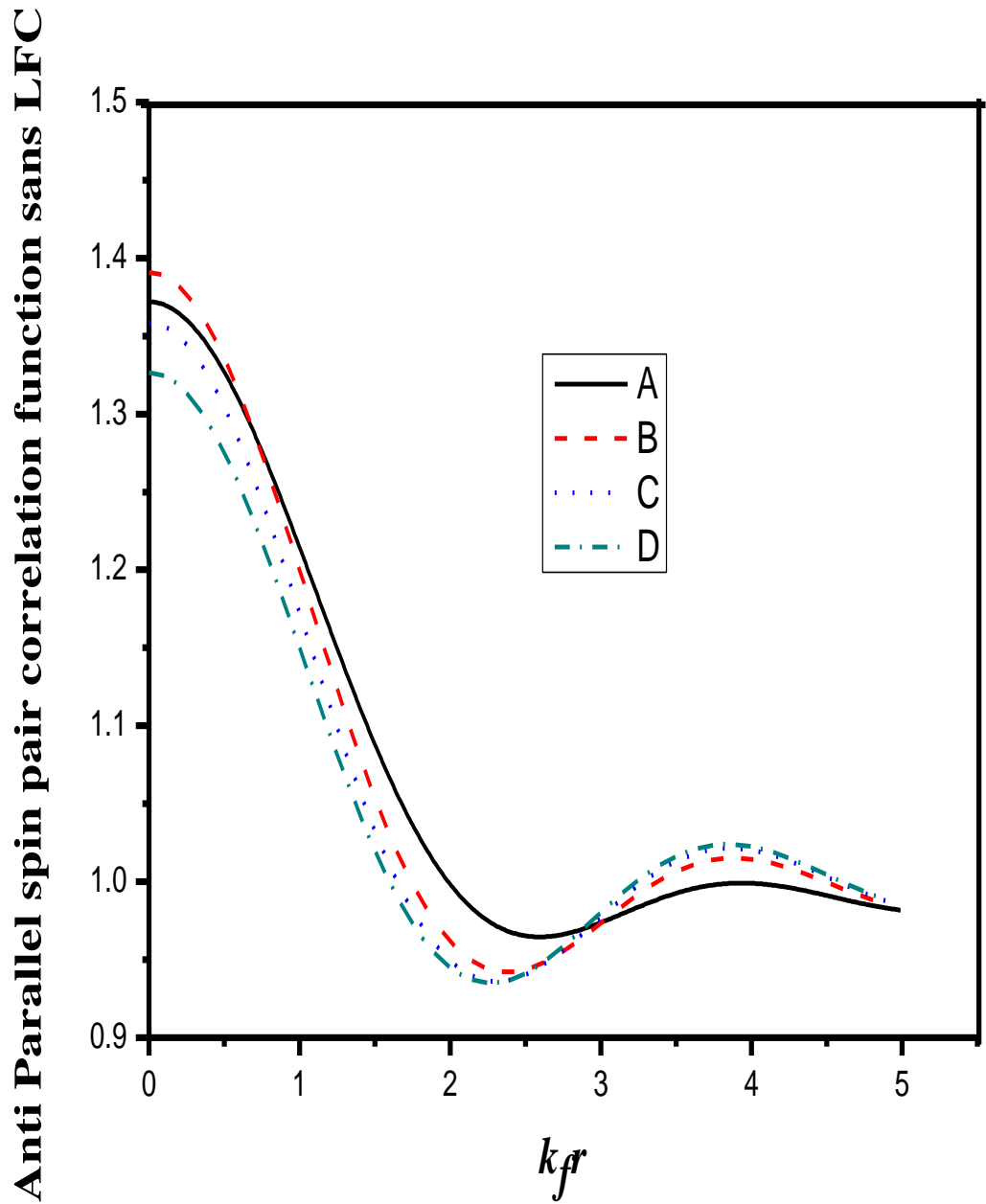


Figure 2.12 Anti parallel spin dimensionless regularised pair correlation function, $g_{\uparrow\downarrow}(k_F \vec{r})$ vs $k_F \vec{r}$, sans LFC, in the curves A, B, C & D, for dimensionless coupling constants $\alpha = 1, 2, 3$ & 4, respectively.

We computed equations (2.17-2.19, 2.21) numerically to obtain self energy, density of screening charge, screened potential and compressibility of SLG. The first three quantities has been also evaluated for Bilayer Graphene (BLG) and compared with that of SLG. The difference in magnitude of $E^{sl}(k)$, $n_s(r)$ and $V_{SCR}(r)$, of SLG, BLG and 2DEG is because of difference in values of intrinsic parameters of three systems, which enter into the quantities through static dielectric function that can be described by $\epsilon(q) = (1 + \beta/q)$ for SLG, BLG and 2DEG. Where β is equal to $4m^*e^2/\epsilon\hbar^2k_f$, which depends on n in case of 2DEG and BLG, while for SLG it is independent of n .

2.3.2 Self Energy

The self-energy is the central quantity for determining the many Fermi liquid parameters. Our computed E^{sl}/e^2k_f from equation (2.17) is plotted as a function of x in figure 2.13 without LFC and in figure 2.14 with the inclusion of LFC. We also computed self-energy of 2DEG and BLG to compare it with that of doped SLG. As is seen from figure 2.13 and figure 2.15, behaviour of computed E^{sl}/e^2k_f of SLG with x is very similar to that of 2DEG and BLG. However, magnitude of E^{sl}/e^2k_f of doped BLG is greater than SLG which in turn is greater than 2DEG. For computing E^{sl} of 2DEG, we have used $m^* = 0.067m_e$ and $\epsilon = 13$. Further to see the effect of LFC on self-energy, we computed E^{sl}/e^2k_f including LFC within HA for doped SLG.

As is seen from figures;

- i. magnitude of self-energy reduces marginally
- ii. downward slope of E^{sl} verses x enhances, especially for $x > 1$, on inclusion of LFC. This suggests that local fields does not play very important role in determination of self-energy in a doped SLG.
- iii. The larger magnitude of screened self energy of BLG than of that of SLG, suggests that the quasiparticle life time for BLG is much larger than that for SLG.

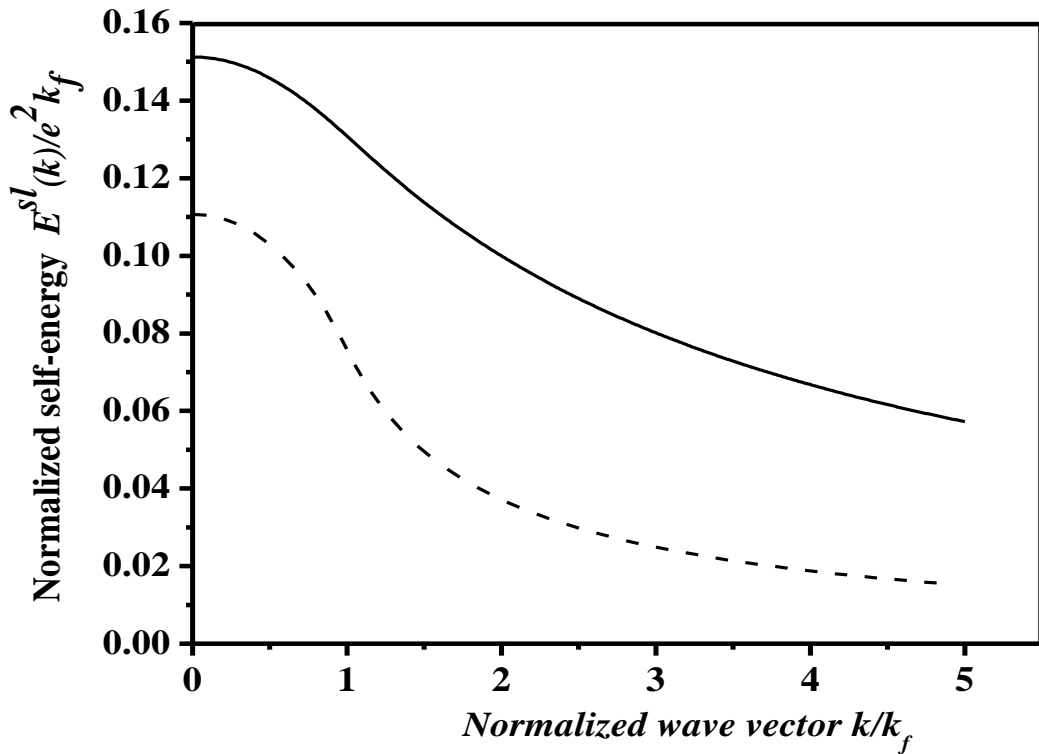


Figure 2.13 Normalized screened self energy, $E^{sl}(k)/e^2k_f$ is plotted against normalized wave vector k/k_f . Solid Curve displays Self energy of graphene while dashed curve is for 2DEG, without LFC.

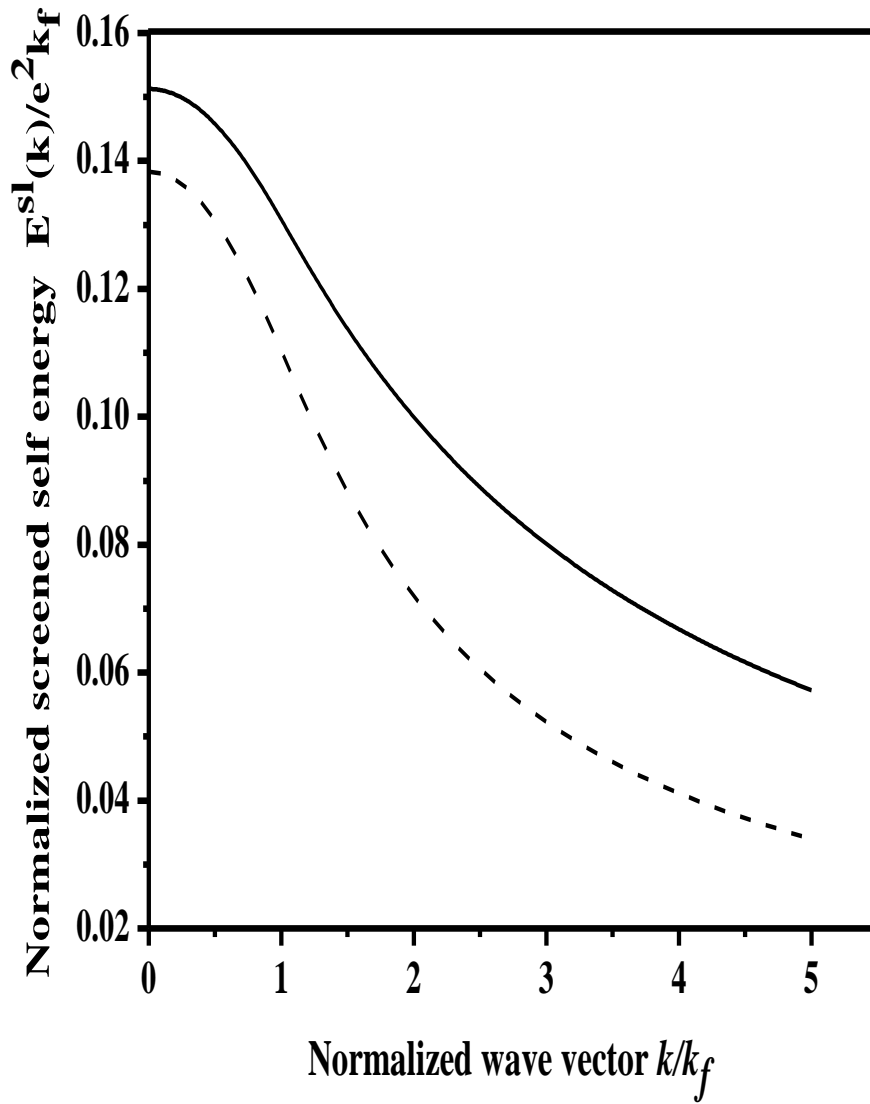


Figure 2.14 Normalized screened self energy, E^{sl}/e^2k_f as a function of k/k_f without LFC (solid line curve) with LFC (dashed line curve).

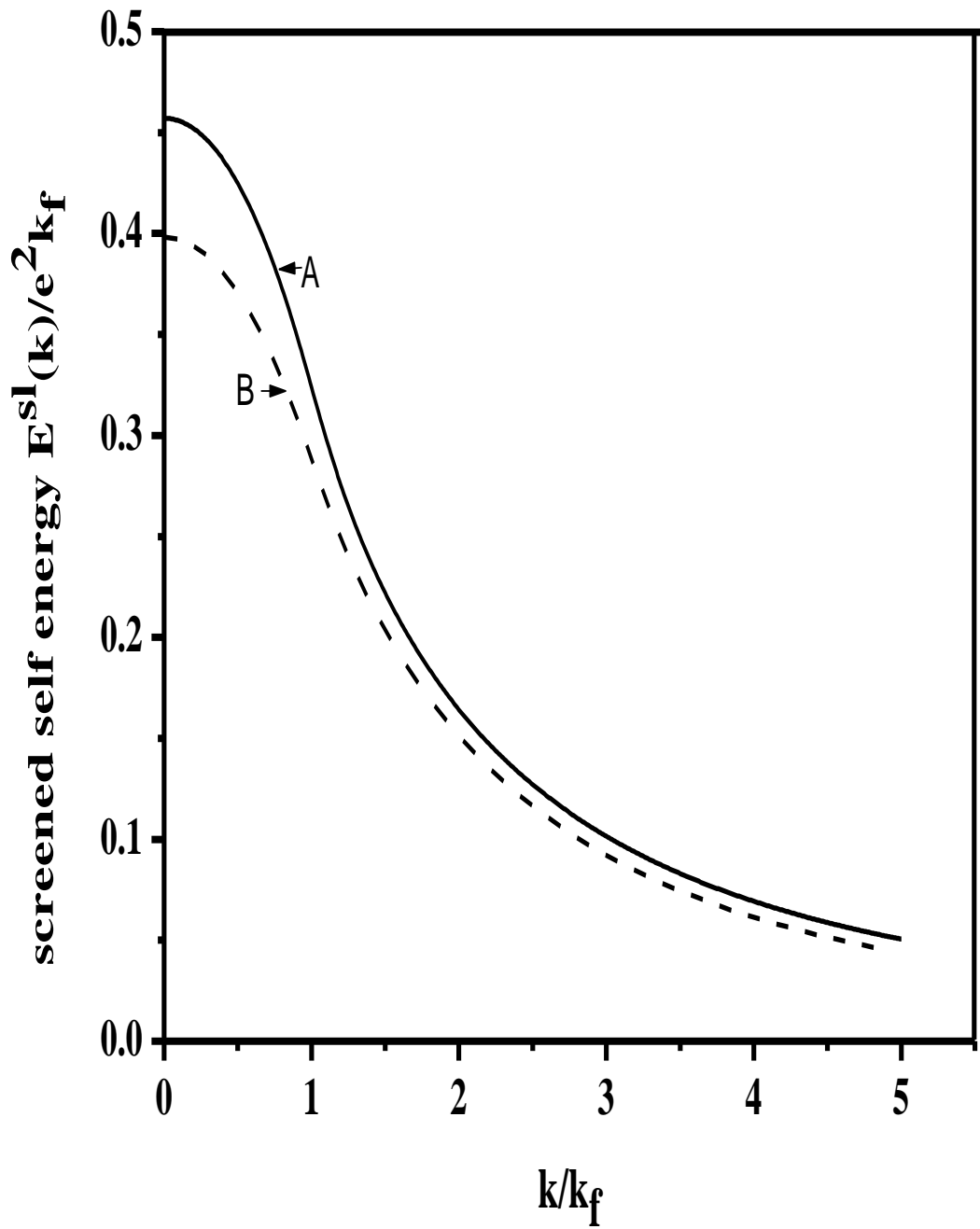


Figure 2.15 Screened self energy for BLG $E^{sl}(k)/e^2 k_f$ versus x Curve-A is for $n = 10^{14} \text{cm}^{-2}$ while Curve-B is for $n = 5 \times 10^{13} \text{cm}^{-2}$

2.3.3 Density of Screening Charge and screened Potential

Our computed $n_s(r)$ is plotted as a function of $k_f r$ in figure 2.16 for two values of α ($=2$ & 4) at fix value of n and in figure 2.17 for two values of n ($n = 4.77 \times 10^{14} \text{cm}^{-2}$ & $8.04 \times 10^{14} \text{cm}^{-2}$) for $\alpha = 4$. Computed $n_s(r)$ is finite for r tending to zero and it exhibits oscillations, which eventually decays for lager values of r . These oscillations are known as Friedel oscillations and are the result of the non-analyticity which occurs because of the discontinuity [9, 42].

As is displayed in figure 2.16, on increasing the value of α for fixed value of n ;

- (i) $n_s(r)$ substantially enhances for lower values of r (close to $r \rightarrow 0$) and
- (ii) Friedel oscillations becomes more pronounced. The behaviour of our computed $n_s(r)$ is very similar to that observed in a Fermi liquid where many body effects influence the amplitude of oscillations which are characterized by power law decay and depend on the strength of the interactions [9].

Figure 2.17, shows that on increasing carrier density at fixed value of α , magnitude of $n_s(r)$ reduces specially for $k_f r$ close to zero and the amplitude of Friedel oscillations decreases. Inclusion of LFC reduces the magnitude of $n_s(r)$ at all r -values and makes it better behaved for $r \rightarrow 0$, as is seen from figure 2.18. Our computed screened potential with the use of equation (2.19) is plotted in figure 2.20. Friedel Oscillations are clearly observed in the potential images which are in good agreement with the experimental work conducted on 2DEG, using low temperature Scanning tunneling microscope [43]. Inclusion of LFC reduces the magnitude of $V_{SCR}(r)$ too and makes it better behaved as is displayed in figure 2.20 Under the RPA approximation, which assumes that the induced charge density is proportional to the total potential, the screened potential oscillates spatially. The observation of

Friedel oscillations in screened potential and screening charge density can be seen as a signature of Fermi liquid state in graphene [44].

The Friedel oscillations can be used to gain insight into the microscopic nature of disorder. We compared our computed $n_s(r)$ and $V_{SCR}(r)$ of doped SLG with that of 2DEG and BLG. It is found that the overall behavior of $n_s(r)$ and $V_{SCR}(r)$ of doped SLG is not very different from that of 2DEG and BLG (figures 2.19 and 2.21), though the nature of charge carriers in two systems is very different [37]. It therefore can be inferred that the linear energy dispersion and chirality of SLG does not significantly influence gross many particle properties.

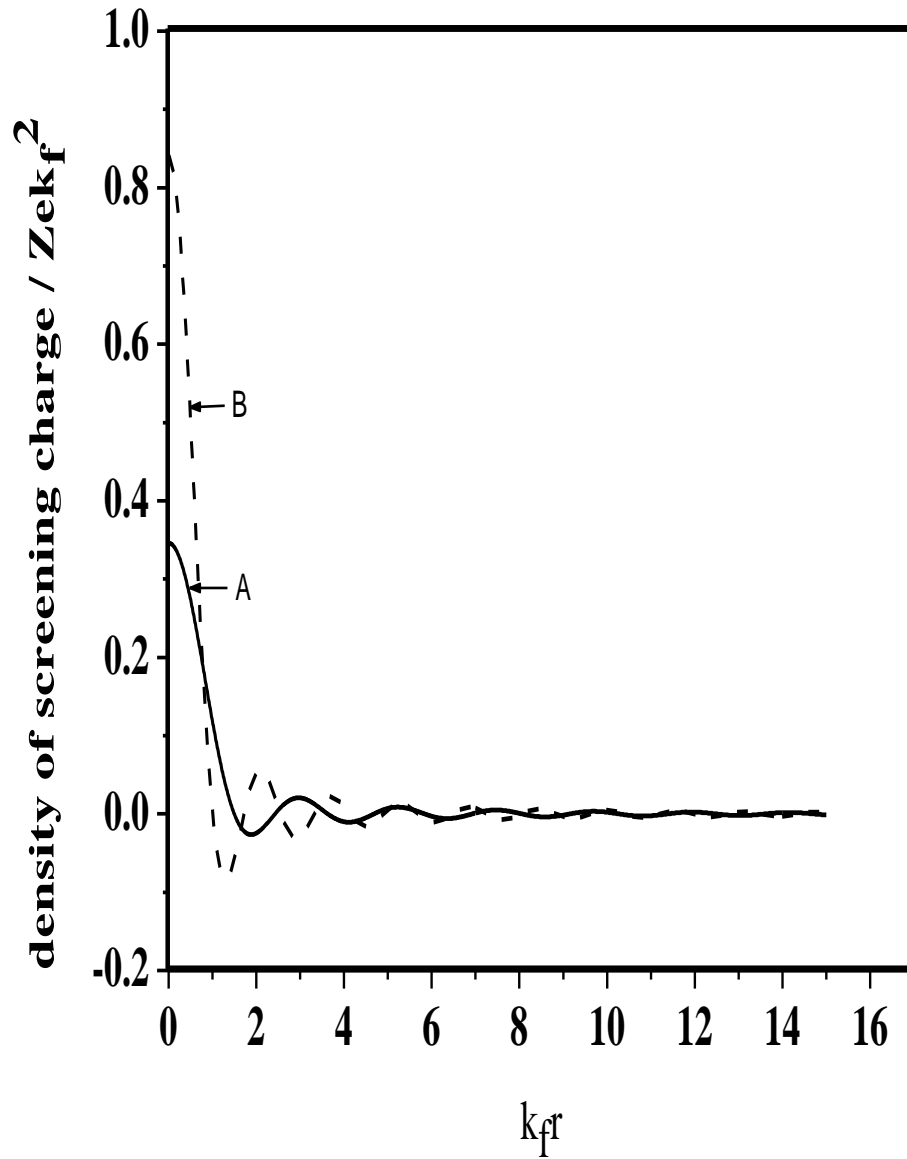


Figure 2.16 Density of screening charge plotted against $k_f r$ for $n = 4.77 \times 10^{14} \text{ cm}^{-2}$ at $\alpha = 2$ (Curve-A) and for $\alpha = 4$ (curve-B).

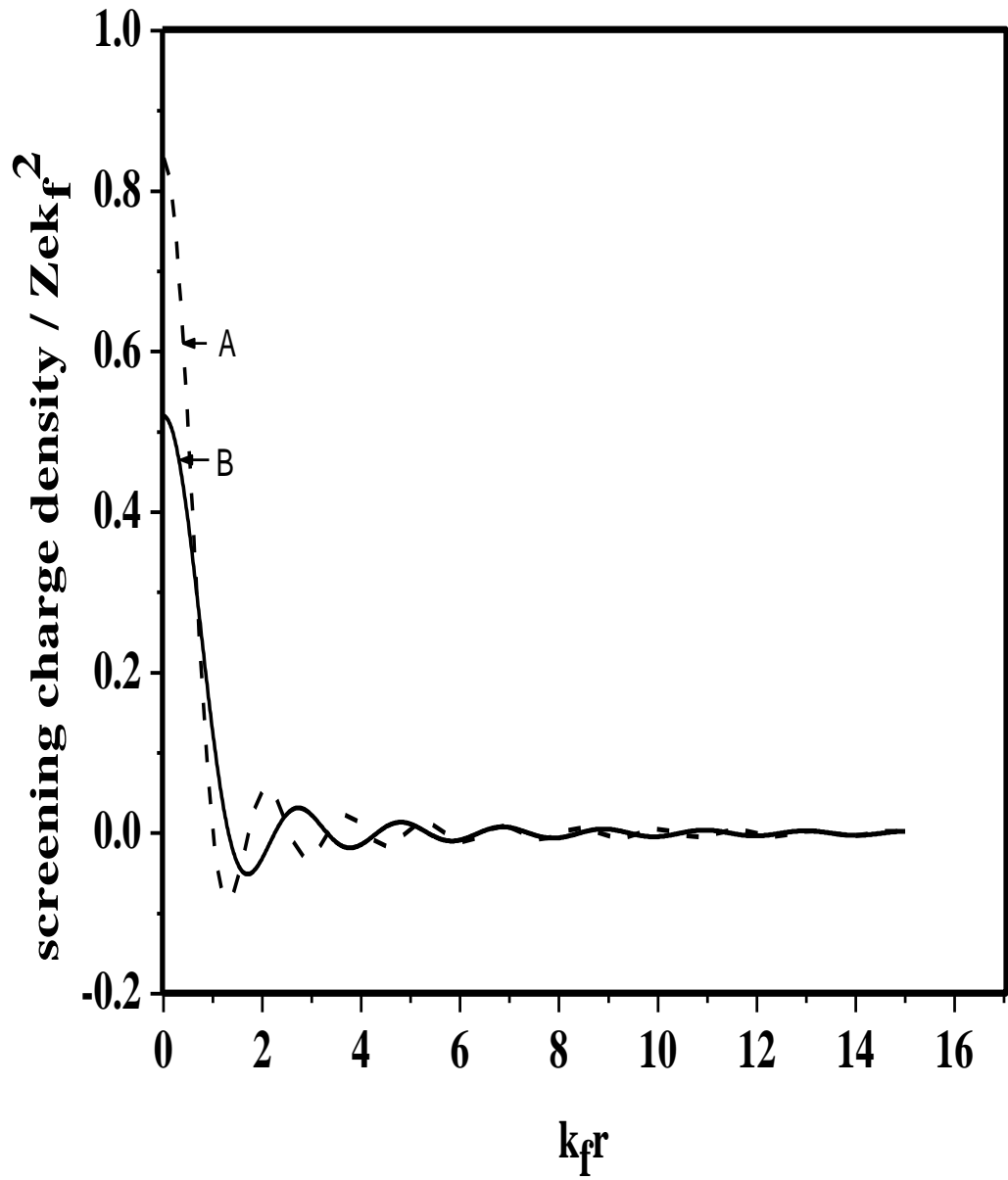


Figure 2.17 Density of screening charge $n_s(r)/Zek_f^2$ plotted against $k_f r$ for SLG for $\alpha = 4$ at $n = 8.04 \times 10^{14} \text{ cm}^{-2}$ (curve-B) and $n = 4.77 \times 10^{14} \text{ cm}^{-2}$ (curve-A).

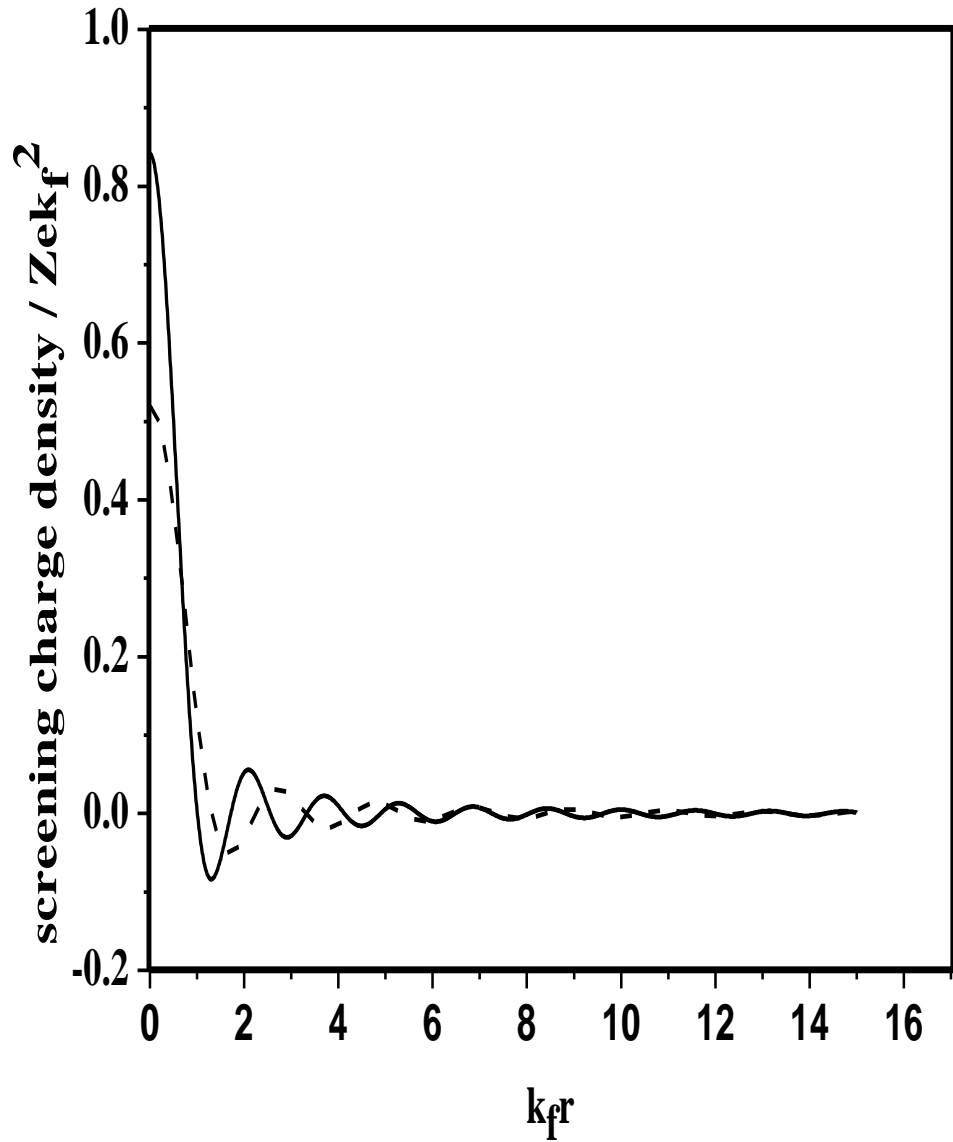


Figure 2.18 Density of screening charge $n_s(r)/Zek_f^2$ with LFC (dashed line) and without LFC (solid line) for $\alpha = 4$ at $n = 8.04 \times 10^{14} \text{ cm}^{-2}$.

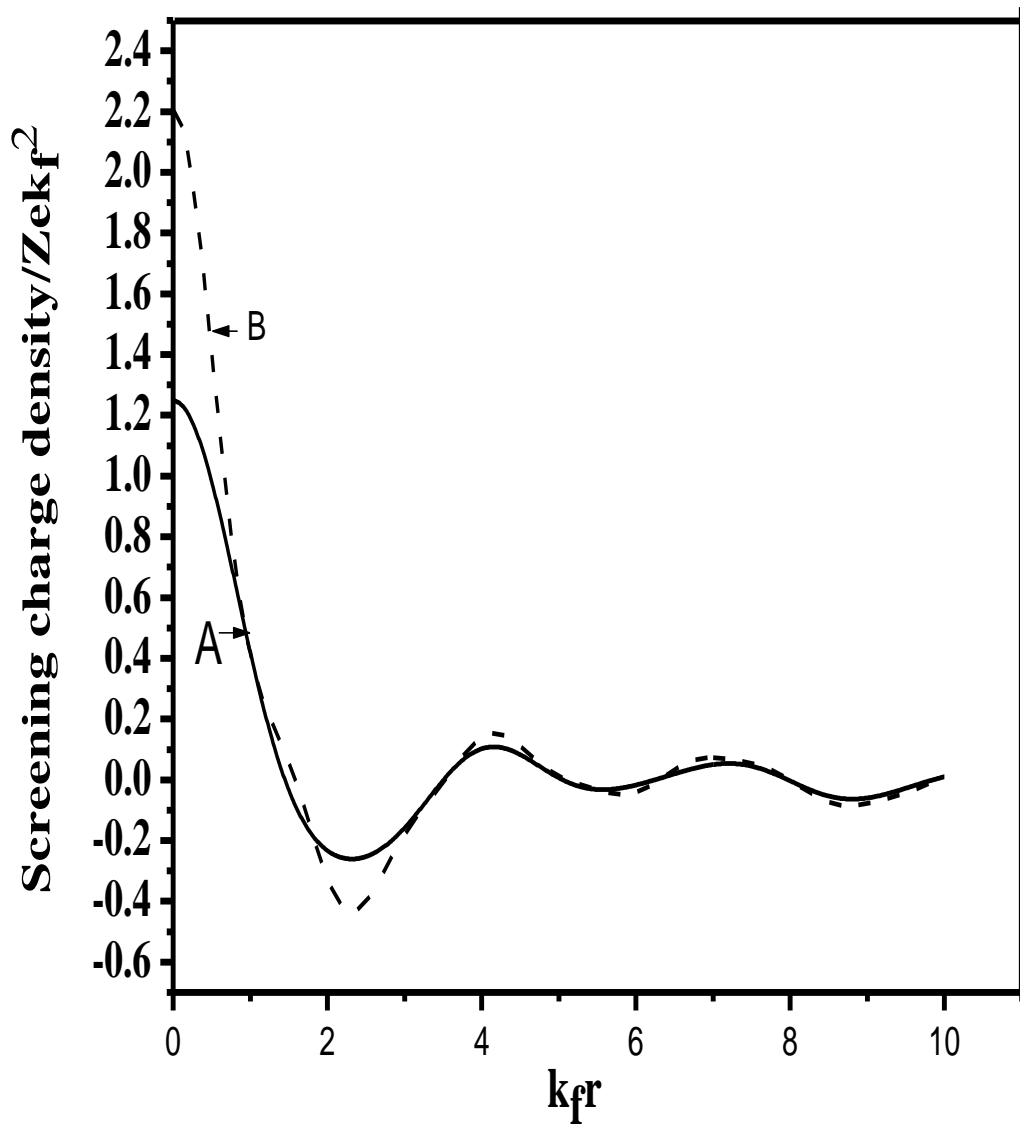


Figure 2.19 Density of screening charge $n_s(r)/Zek_f^2$ versus $k_f r$ for BLG Curve-A is for $n = 10^{14} \text{ cm}^{-2}$ while Curve-B is for $n = 5 \times 10^{13} \text{ cm}^{-2}$

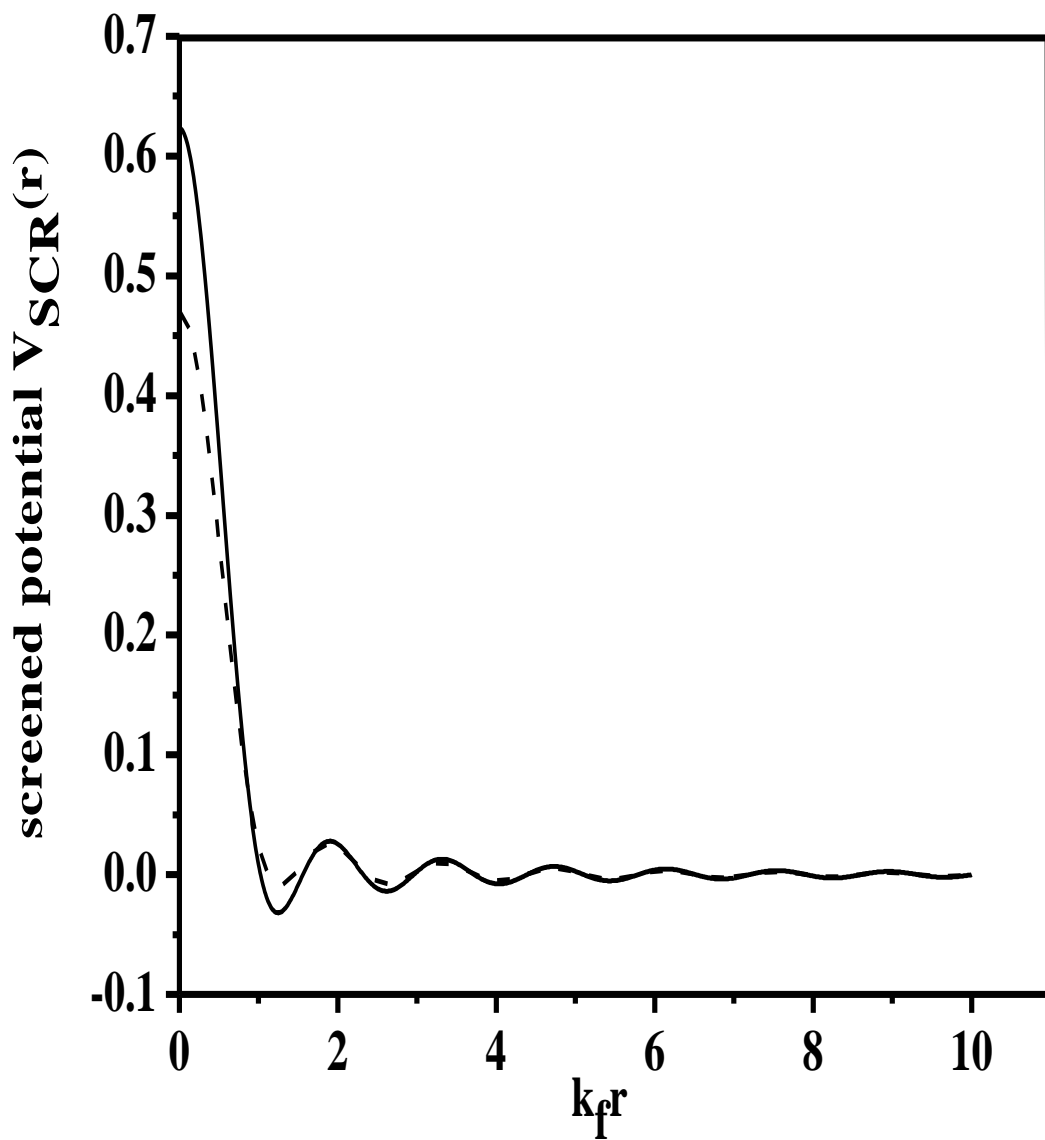


Figure 2.20 Screened potential $V_{SCR}(r) \rightarrow k_f r$; with LFC(dashed line), without LFC (solid line)

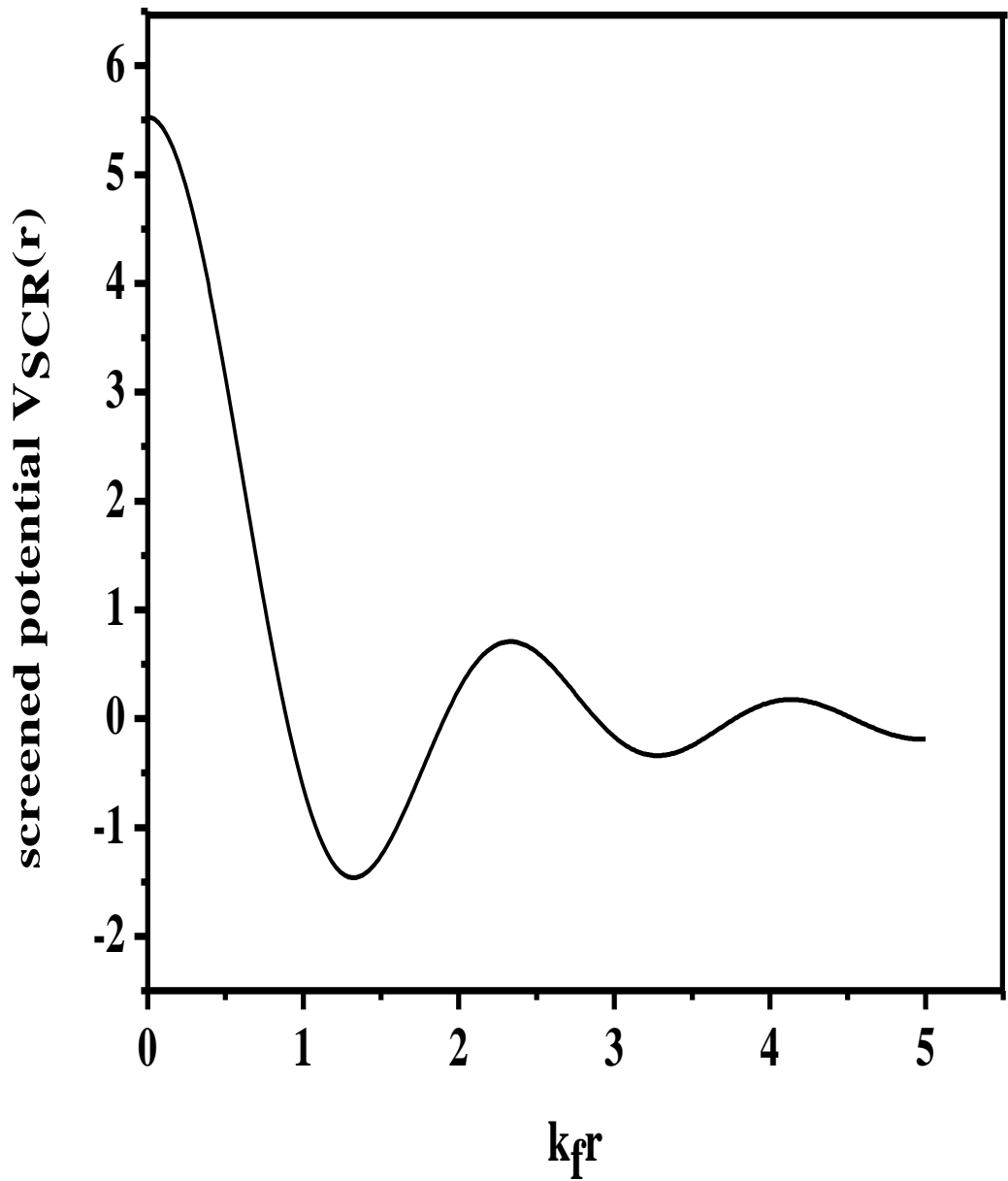


Figure 2.21 Screened Potential $V_{SCR}(r)$ versus $k_f r$ for BLG for $n = 10^{14} cm^{-2}$

2.3.4 Compressibility

We computed $g(r)$ as a function of n at different α -values. To study the pair distribution function as a function of n we took $n = z \times 10^{14} \text{ cm}^{-2}$ at a fixed $r = 1 \times 10^{-7} \text{ cm}$. Further for computation we take dimensional less quantity q/q_0 , where $q_0 = 1 \times 10^7 \text{ cm}^{-1}$. Our computed results are displayed in figure 2.22 for different values of α . For all values of α , computed $g(r, z)$ as a function of carrier density saturates at higher values of z , as is exhibited in the figure. Figure 2.22, clearly suggests that the variation of $g(r, z)$ with n is roughly zero over the experimentally observed range of n in doped SLG. Looking at figure 2.22 and Equation (2.20), we can conclude that exchange and correlation terms make negligible contribution to compressibility in SLG, as has been observed in experimental results on compressibility of SLG [33].

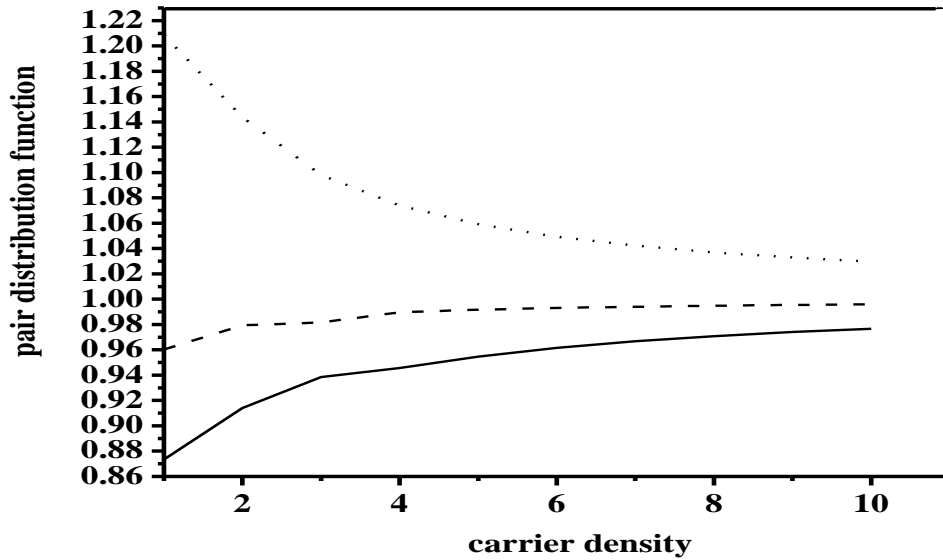


Figure 2.22 Pair distribution function $g(r, z) \rightarrow z$ for $\alpha = 1$ (solid line), $\alpha = 2$ (dotted line) and $\alpha = 3$ (dashed line)

2.4 References

1. Y. Barlas, T. Pereg-Barnea, M. Polini, R. Asgari and A. H. Mac Donald 2007 Phys. Rev. Lett. **98** 236601
2. M. Polini, R. Asgari, Y. Barlas, T. Pereg-Barnea, and A. H. Mac Donald 2007 Solid State Commun. **143** 58
3. A. Qaiumzadeh and R. Asgari 2009 New J. Phys. **11** 095023
4. K. W. Shung 1986 Phys. Rev. B **34** 979
5. J. Gonzalez, F. Guinea and M A H Vozmediano 1994 Nucl. Phys. B **424** 595
6. T. Ando 2006 J. Phys. Soc. Jpn **75** 074716
7. X. Wang and T. Chakraborty 2007 Phys. Rev. B **75** 033408
8. V. N. Kotov, V. M. Pereira and B. Uchoa 2008 Phys. Rev. B **78** 075433
9. B. Wunsch, T. Stauber , F. Sols and F Guinea 2007 New J. Phys. **8** 318
10. E H Hwang, S D Sarma 2007 Phys. Rev. B **94** 136602
11. E H Hwang, S D Sarma 2009 Phys. Rev. B **79** 165404
12. P K Pyatkovskiy 2009 J.Phys.: Condens. Matter **21** 025506
13. S Gangadhariah, A M Farid and E G Mischenko 2008 Phys. Rev. Lett. **100** 166802
14. J Sabio , J Nilsson , A H Castro Neto 2008 Phys. Rev. B **78** 075410
15. O Vafek 2007 Phys. Rev. Lett. **98** 216401
16. M R Ramezanali, M Vazifeh, R Asgari ,M Polini and A H MacDonald 2009 J.Phys. A:Math. Theor. **42** 214015
17. A Qaiumzadeh and R Asgari 2009 Phys. Rev. B **79** 075414
18. K F Allison, D Baka, I Radovic, Lj Hadzievski and Z L Miskovic 2009 Phys. Rev. B **80** 195405
19. Gori-Giorgi and P F Sacchetti 2000 Phys. Rev. B **61** 7353 and references there in.
20. G D Mahan 1990 *Many Particle Physics* 2nd edn (New York: Plenum)
21. M W C Dharma-wardana 2007 Phys.Rev. B **75** 075427
22. K Shiyuza 2008 Phys. Rev. B **77** 075419
23. E H Hwang, Ben Yu-Kuang Hu, S D Sarma *Physica E* (2008) **40** 1653-1655
24. S D Sarma, E H Hwang, and W K Tse, Phys. Rev. B (2007) **75**, 121406(R)
25. M Calandra and F Mauri, Phys. Rev. B (2007) **76**, 205411 ;

26. C H Park, F Giustino, M L Cohen, and S G Louie, *Phys. Rev.Lett.* (2007) **99**, 086804;
27. W K Tse and S D Sarma, *ibid* (2007). **99**,236802.
28. N W Ashcroft and N D Mermin, *Solid State Physics* (Saunders College, Philadelphia,1976)
29. Ivan S. Terekov, Alexander I. Milstein, Valeri N. Kotov, and Oleg P.Sushkov *Phy Rev Lett* 100 (2008),076803;
30. A V Shytov, M I Katsnelson, and L S Levitov, *Phys. Rev.Lett.* (2007) **99**, 236801
31. E H Hwang, S D Sarma, *Phys. Rev. B* (2007) **75**, 205418
32. A H Castro Neto, F Guinea, N M Peres, K S Novoselov and A K Geim 2009 *Rev. Mod. Phys.* **81** 109
33. J Martin, N Akerman, G Ulbricht, T Lohmann, J H Smet, Klitzing K von, and A Yacoby, *Nat. Phys.* (2008) **4** , 144.
34. D S L Abergel, P Pietilainen, and T Chakraborty , *Phys. Rev. B* (2009) **80**, 081408(R).
35. S S Z Ashraf, A C Sharma and K N Vyas 2007 *J.Phys.: Condens. Matter* **19** 306201
36. G F Giuliani and G Vignale 2005 *Quantum Theory of the Electron Liquid* (Cambridge University Press, Cambridge)
37. D.S.L. Abergel, V. Apalkov, J. Berashevich, K. Ziegler, and T. Chakraborty, *Advances in Physics*, **59: 4**, 261 — 482 (2010).
38. N M R Peres, F Guinea and A H Casto Neto 2005 *Phys. Rev. B* **72** 174406
39. Gori-Giorgi Paola, Moroni Saverio and Blachelet Giovanni B. 2004 *Phys. Rev. B* **70** 115102
40. A Qaiumzadeh and R Asgari 2009 *Phys. Rev. B* **80** 035429
41. B Tanatar and C Bulutay 1999 *Phys. Rev. B* **59** 15019
42. Vadim V Cheianov and Vladimir I. Fal'ko *Phy. Rev. Lett.* (2006) **97**, 226801
43. Masanori Ono *et al. Applied Surface Science* (2009) **256** 469-474
44. Simion George E. and Giuliani Gabriele F. *Phys. Rev. B* (2005) **72**, 045127